




Global dynamics of Chua Corsage Memristor circuit family: fixed-point loci, Hopf bifurcation, and coexisting dynamic attractors

Zubaer Ibna Mannan · Shyam Prasad Adhikari ·
Hyongsuk Kim  · Leon Chua

Received: 24 February 2019 / Accepted: 7 January 2020 / Published online: 7 February 2020
© Springer Nature B.V. 2020

Abstract This paper presents an in-depth and rigorous mathematical analysis of a family of nonlinear dynamical circuits whose only nonlinear component is a *Chua Corsage Memristor (CCM)* characterized by an explicit seven-segment piecewise-linear equation. When connected across an external circuit powered by a DC battery, or a sinusoidal voltage source, the resulting circuits are shown to exhibit four asymptotically stable *equilibrium points*, a unique stable *limit cycle* spawn from a supercritical *Hopf bifurcation* along with three static attractors, four *coexisting dynamic attractors* of an associated *non-autonomous nonlinear differential equation*, and four corresponding *coexisting pinched hysteresis loops*. The *basin of attractions* of the above static and dynamic attractors is derived numerically via *global nonlinear analysis*. When driven by a battery, the resulting *CCM circuit* exhibits a *contiguous fixed-point loci*, along with its *DC V-I curve* described analytically by two explicit *parametric equations*. We also proved the *fundamental feature of the*

edge of chaos property; namely, *it is possible to destabilize a stable circuit* (i.e., without oscillation) and make it *oscillate*, by merely adding a *passive circuit element*, namely $L > 0$. The *CCM circuit family* is one of the few known example of a strongly nonlinear dynamical system that is endowed with numerous coexisting static and dynamic attractors that can be studied both experimentally, and mathematically, via exact formulas.

Keywords Corsage Memristor · Fixed-point loci · Phase portrait · Basin of attraction · Local activity · Hopf bifurcation · Coexisting dynamic attractors

1 Introduction

Nonlinear dynamical systems are of interest in scientific research field as most of the systems in nature are inherently nonlinear [1–3]. Various nonlinear dynamical systems have multiple coexisting attractors, and the properties (such as fixed points, limit cycles, toruses, and chaotic) of these attractors depend upon the embedded parameters and initial conditions. Starting from a set of initial conditions, the basin of attraction of each such attractor exhibits a long-time transitional behavior approaching toward the attractors. Thus, the qualitative behavior of the long-time motion of a given nonlinear dynamical system depends upon the initial conditions [4, 5]. The dynamic behavior of a nonlinear system can be verified by analyzing its behavior based on the theorem of bifurcation and chaos which is highly dependent

Z. I. Mannan · S. P. Adhikari · H. Kim (✉)
Division of Electronics and Information Engineering, and
Intelligent Robot Research Center, Chonbuk National
University, Jeonju, Jeonbuk 567-54896, Republic of Korea
e-mail: hskim@jbnu.ac.kr

L. Chua
Department of Electrical Engineering and Computer Sciences,
University of California, Berkeley, CA 94720-1770, USA

on initial conditions of the systems. Moreover, *complex phenomena* and *information processing* tend to emerge over the parameter ranges of a system, operating on, or near the neighborhood of its *edge of chaos* domain [6, 7]. Memristor is regarded as one of the most prominent element to exhibit both complex phenomena (such as oscillation and chaos [4–9]) and information processing (such application in neural network [10–12], resistive switching memory [13], and artificial intelligence [14]). Recently, numerous research activities have been conducted to exploit the nonlinear dynamical attributes of memristive systems in electronic circuits.

This paper presents an in-depth and rigorous nonlinear analysis of the Chua Corsage Memristor¹ (CCM). The versatile CCM is a *piecewise-linear (PWL) multi-state memory device* with the following state-dependent Ohm’s law and state equation [15]:

State-Dependent Ohm’s Law

$$i = G(x) v, \tag{1}$$

$$\text{where } G(x) = G_0 x^2, \tag{2}$$

State Equation

$$dx/dt = f(x, v) = f(x) + v, \tag{3}$$

where

$$f(x) = 33 - x + |x - 6| - |x - 12| + |x - 20| - |x - 30| + |x - 42| - |x - 56|, \tag{4}$$

and x , v , and i denote the memristor state, voltage, and current, respectively, as shown in Fig. 1. The intrinsic memductance scale of the memristor is fitted with scaling constant G_0 . In this paper, we choose $G_0 = 1$ so that the parameters of the small-signal equivalent circuit of the CCM will not be excessive.

This paper presents an in-depth and rigorous nonlinear analysis of three members of the Chua Corsage Memristor (CCM) circuit family, where the CCM is driven by the external active circuits shown in Fig. 2:

External Circuit 1 A DC voltage source (battery) whose voltage $v = E$ is tuned over the entire real line, i.e., $-\infty < v < \infty$.

The resulting loci of the *steady state* (after the transient tends to zero) $x = X$, plotted as a function of constant voltage $v = V$ (dubbed the *fixed-point loci*),

¹ The Chua Corsage Memristor is not a hypothetical device, but can be built using off-the-shelf components [15].

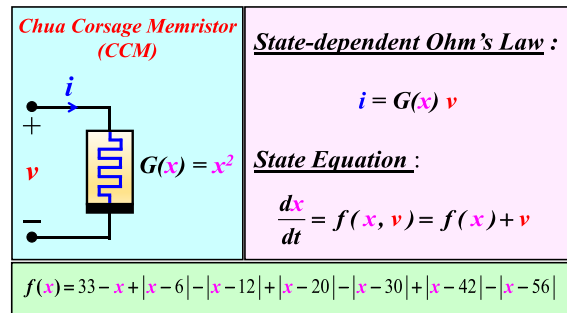


Fig. 1 Definition of the Chua Corsage Memristor (CCM) with $G_0 = 1$

is proved in Sect. 2.3 to cover the entire real line— $-\infty < X < \infty$, as the DC (constant) voltage is tuned from $V = -\infty$ to $V = +\infty$. The corresponding steady-state current I can be calculated from the state-dependent Ohm’s law of the CCM. When plotted in the I vs. V plane, the fixed-point loci is proved in Sect. 2.3 to be a multi-valued but contiguous curve—called the DC V – I curve of the CCM.

External Circuit 2 A DC voltage source (with fixed voltage $v = V_{DC}$) in series with an inductor whose inductance $L = L^*$ (derived via Chua’s oscillation formula) gives rise to a stable oscillation via Hopf bifurcation.

A rigorous phase plane analysis supported by a detailed *phase portrait* is presented in Sect. 5 along with a unique stable limit cycle and its *basin of attraction*.

External Circuit 3 An AC sinusoidal voltage source $v_s(t) = A \sin(\omega t)$ is applied across the CCM. Over a wide range of amplitude A and frequency ω , we show that, depending on the *initial state* $x(0)$, the CCM circuits exhibit four distinct *stable periodic* steady-state response $x_a(t)$, $x_b(t)$, $x_c(t)$, and $x_d(t)$. The range of the initial state $x(0)$ which converges to a particular periodic steady-state response $x_j(t)$, $j \in \{a, b, c, d\}$, is called the *basin of attraction* $B_j(0)$ of the *dynamic attractor*² $x_j(t)$. It is called an *attractor* because any trajectory with an initial state originating from inside the *basin of attraction* $B_j(0)$ converges to, or is

² We appended the adjective “dynamic” to differentiate it from *static* attractors (i.e., equilibrium states) of *autonomous* systems, since the CCM circuit 3 is driven by a time-varying input signal $v_s(t)$, resulting in a *non-autonomous* nonlinear differential equation, and is therefore never in equilibrium.

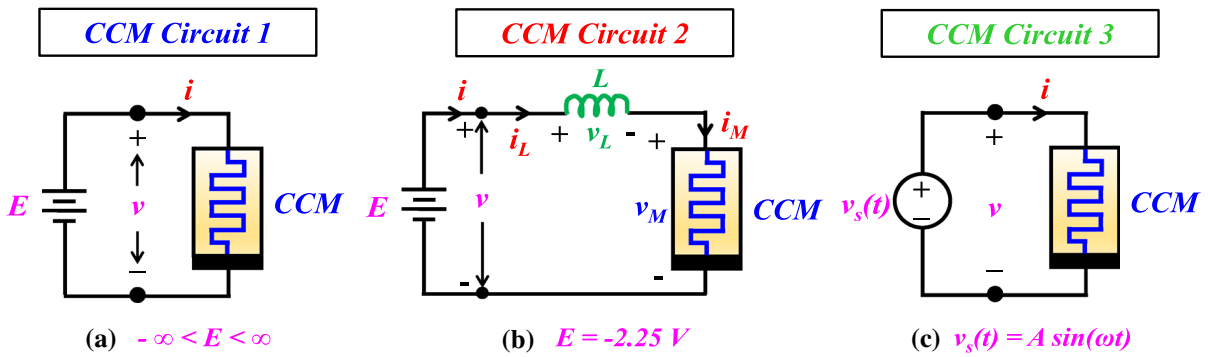


Fig. 2 Three Chua Corsage Memristor (CCM) circuits. **a** *CCM Circuit 1*: The loci of (I, V) in i vs. v plane, as the DC voltage E is tuned from $E = -\infty$ to $E = +\infty$, is called the *DC V-I curve* of the *CCM*. **b** *CCM Circuit 2*: With $E = -2.25$ V and $L = L^* = 355.5$ mH, the *CCM Circuit 2* is described by an *autonomous* system of two nonlinear ordinary differential equations, whose phase portrait shows an *unique stable limit cycle* along with *three asymptotically stable equilibrium points* in the i_L vs. x phase plane. **c**

CCM Circuit 3: The *CCM* is driven by a *periodic sinusoidal voltage source* $v_s(t) = A \sin(\omega t)$, where $A = \{1 \text{ V}, 3 \text{ V}\}$, $\omega = \{0.02\pi \text{ rad/s}, 0.1\pi \text{ rad/s}, 0.2\pi \text{ rad/s}, \pi \text{ rad/s}, 2\pi \text{ rad/s}, 10\pi \text{ rad/s}, 20\pi \text{ rad/s}\}$. The *CCM Circuit 3* is described by a *non-autonomous* nonlinear differential equation. The steady-state response of the state variable $x(t)$ is calculated with *four initial states* $x_a(0), x_b(0), x_c(0)$, and $x_d(0)$, each giving rise to a distinct periodic steady-state response, dubbed a *dynamic attractor*

attracted by, the periodic steady-state response $x_j(t)$, $j \in \{a, b, c, d\}$.

The existence of the above *four coexisting dynamic attractors* $x_a(t), x_b(t), x_c(t)$, and $x_d(t)$ with explicit formulas, along with their basins of attraction, is destined to be a textbook example for future researchers on non-autonomous systems.

For each attractor $x_j(t)$, $j \in \{a, b, c, d\}$, one can trivially calculate via Eq. (1) the corresponding steady-state current $i_j(t)$ of the *CCM*. When plotted in the i vs. v plane, with time t as parameter, the corresponding loci are proved to be a *contiguous pinched hysteresis loop*, as illustrated in Table 1. The *four coexisting pinched hysteresis loops* of the *CCM*, along with their *basins of attraction*, are a surprising new result of this paper.

Table 1 shows four *steady-state* (after the transient tends to zero) *pinched hysteresis loops* of the *CCM Circuit 3* for amplitude $A = 3$ V and frequency $\omega = 0.2\pi$ rad/s. Figure 3a shows an evolution toward the steady-state, and Fig. 3b shows the pinched hysteresis loops when the *CCM Circuit 3* is driven by $v_s(t) = A \sin(\omega t)$, where $A = 3$ V and $\omega = \{1 \text{ rad/s}, 10 \text{ rad/s}, 20 \text{ rad/s}, \text{ and } 100 \text{ rad/s}\}$.

The main contributions of this paper are as follows:

- We present an in-depth and rigorous mathematical analysis of a family of nonlinear dynamical circuits whose only nonlinear component is a *Chua Corsage Memristor (CCM)* characterized by an explicit

seven-segment piecewise-linear equation. Unlike most of the existing various nonlinear systems with disconnected DC $V-I$ curves, the *CCM (CCM Circuit 1)* exhibits a complicated but *contiguous DC V-I loci* induced by the seven equilibrium states which can be expressed analytically by two exact explicit *parametric* equations.

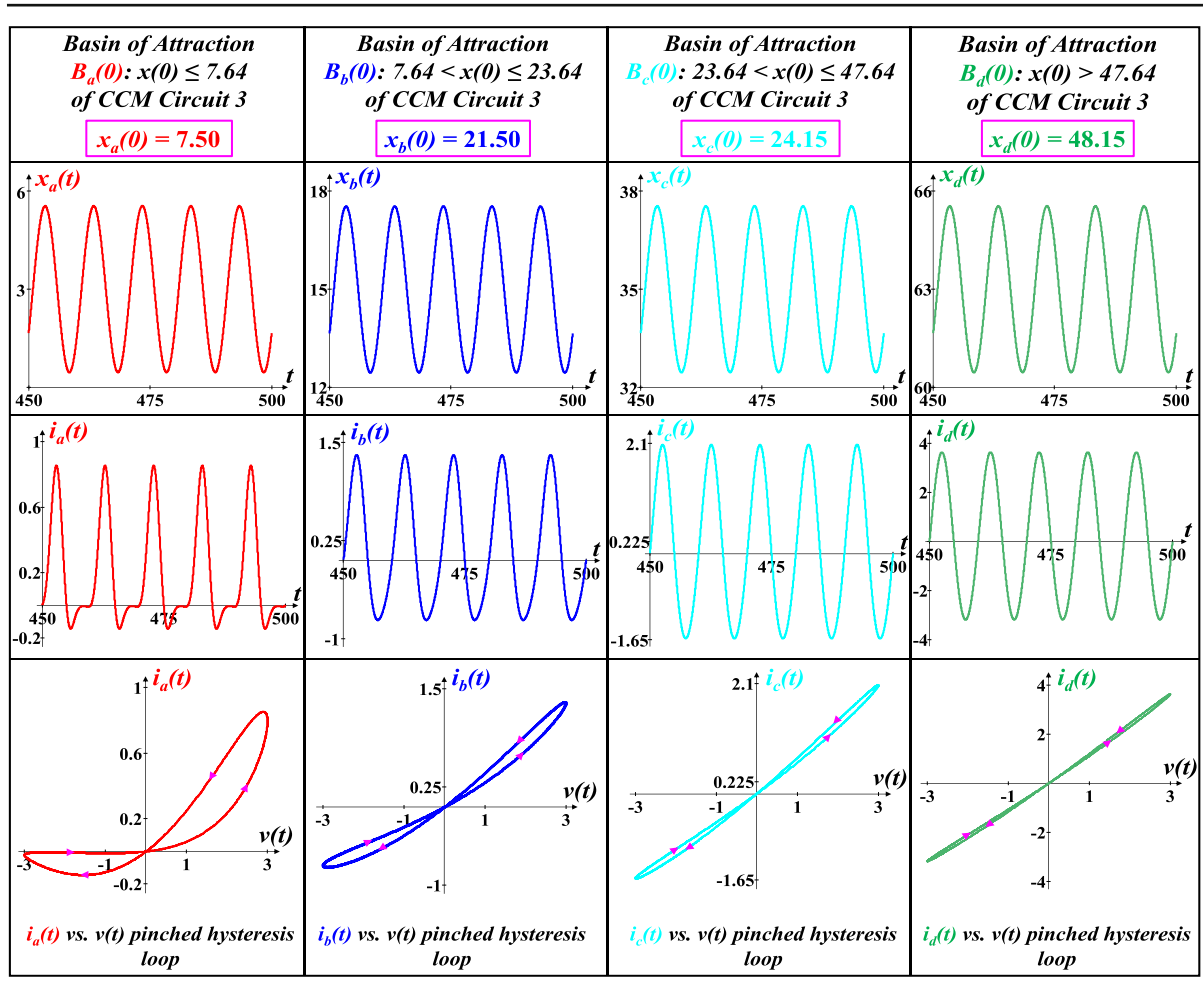
- We proved the *fundamental feature of the edge of chaos property*³ by connecting the *CCM* in series with an appropriate choice of battery voltage $V = V^*$, and inductance $L = L^*$ (i.e., *CCM Circuit 2*) which exhibits a unique stable *limit cycle* spawn from a supercritical *Hopf bifurcation* along with three static attractors in phase plane.
- Another exciting discovery in this paper is that, when driven by $v = A \sin(2\pi ft)$, the *non-autonomous ODE* of *CCM (CCM Circuit 3)* exhibits four distinct *periodic solutions* (namely, $x_a(t), x_b(t), x_c(t)$, and $x_d(t)$) along with four distinct *coexisting pinched hysteresis loops*, whose corresponding *basins of attraction* were precisely calculated.

The rest of the paper is organized as follows: Various attributes of the *CCM* circuits are introduced in Sect. 2. In Sect. 3, the design and in-depth analysis of a *CCM*

³ *Edge of Chaos Property*: It is possible to destabilize a stable circuit (i.e., without oscillation) and make it oscillate, by merely adding a *passive circuit element* ($L > 0$).

Table 1 Basins of attraction of the four dynamic attractors of the CCM Circuit 3, along with their associated coexisting pinched hysteresis loops with sinusoidal excitation $v_s(t) = A \sin(\omega t)$, where $A = 3$ V and $\omega = 0.2\pi$ rad/s. The steady-state response

$x_j(t)$, $j \in \{a, b, c, d\}$, of CCM Circuit 3 for four initial states $x_j(0)$ and its associated steady-state current $i_j(t)$, when plotted in the $i_j(t) - v(t)$ plane, are pinched hysteresis loops



oscillator circuit are presented. The Hopf bifurcation analysis, which gives rise to a *unique stable* limit cycle, is given in Sect. 4. Section 5 presents a detailed analysis of the *phase portrait* of the CCM oscillator, including the location of limit cycle and three asymptotically stable equilibrium points $Q_3, Q_5,$ and Q_7 (*attractors*) and four unstable equilibrium points $Q_1, Q_2, Q_4,$ and Q_6 (*repellers*). The basins of attraction of the limit cycle and three attractors are clearly shown in the phase portrait. Section 6 shows four coexisting pinched hysteresis loops induced by the four coexisting dynamic attractors shown in Table 1, along with their basins of attrac-

tion. The final Sect. 7 is devoted to some concluding remarks.

2 Dynamic route map, parametric representation of contiguous multi-valued DC $V-I$ curve of the CCM, fixed-point loci, and small-signal model

2.1 Dynamic route map of the CCM

In the parlance of nonlinear circuit theory, any curve $f(x, v)$ plotted in the phase plane, e.g., $(dx/dt$ vs. $x)$

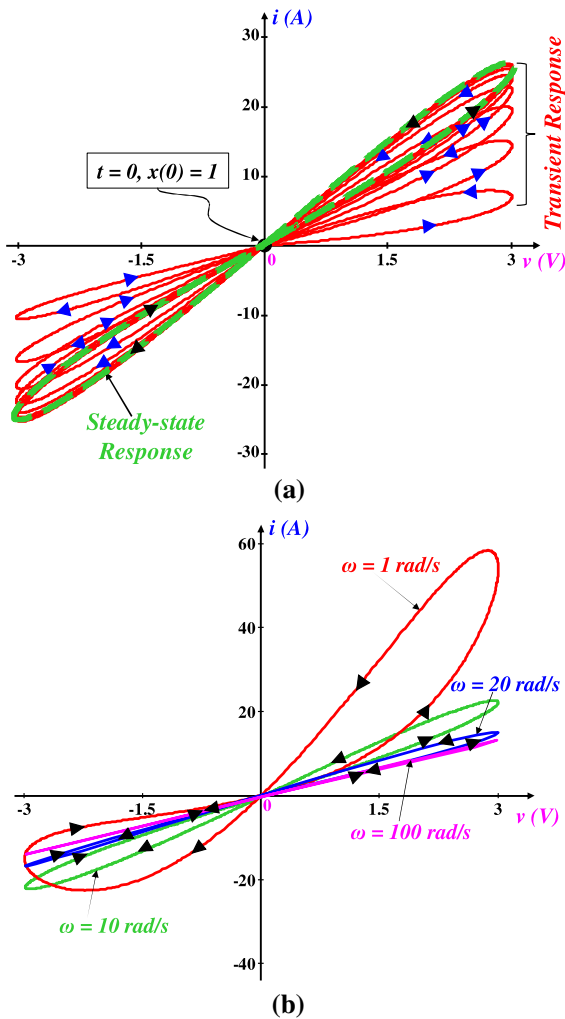


Fig. 3 Signature of the CCM when driven by a sinusoidal input voltage $v_s(t) = A \sin(\omega t)$, where $A = 3 \text{ V}$ and initial state $x(0) = 1$. **a** Illustration of the identical zero-crossing phenomenon with frequency $\omega = 10 \text{ rad/s}$. Observe each lobe of the hysteresis loop always passes through the origin whenever $v_s(t) = 0$, as the transient component decreases over time. **b** Four frequency-dependent steady-state pinched hysteresis loops computed with frequencies $\omega = \{1 \text{ rad/s}, 10 \text{ rad/s}, 20 \text{ rad/s}, \text{ and } 100 \text{ rad/s}\}$

plane, along with the *direction of motion* from the representative points is called a *dynamic route* where it prescribes the dynamics of the defining scalar nonlinear differential equation [16, 17]. In spite of its simplicity, the *dynamic route map (DRM)* is the most powerful and ideal tool for analyzing the dynamics of any first-order differential equation $dx/dt = f(x, v)$ because of its predictability regarding the evolution of any initial state

with increasing time [18]. The dynamic route map of the CCM Circuit 1 is shown in Fig. 4 for input voltages $v = V = \{-9 \text{ V}, -7 \text{ V}, -5 \text{ V}, -3 \text{ V}, 0 \text{ V}, 3 \text{ V}, 5 \text{ V}, 7 \text{ V}, 9 \text{ V}\}$. Observe that for any applied nonzero positive voltage ($v = +V_A$), the red curve $f(x, 0)$ is translated upward by V_A units. Conversely, for any nonzero negative voltage ($v = -V_A$), the red curve $f(x, 0)$ is translated downwards by V_A units, as shown in Fig. 4. As an example, for $v = +3 \text{ V}$ the corresponding DRM for $f(x, 3)$ (blue curve) is obtained by translating the red curve (parameterized by $v = 0$) upward by three units. In contrast, for $v = -7 \text{ V}$, the DRM for $f(x, -7)$ (burgundy curve) is obtained by translating the red curve $f(x, 0)$ downward by seven units, as shown in Fig. 4.

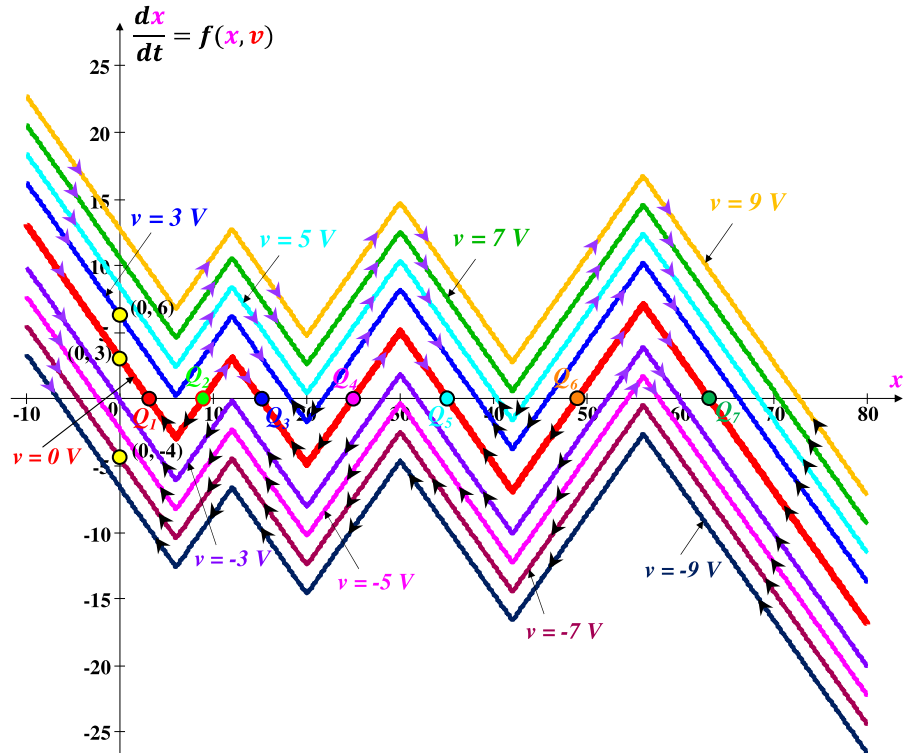
2.2 Power-off plot (POP) of the CCM

The short-circuited ($v = 0$) dynamic route, also known as *Power-off plot (POP)* [17] of the CCM, is the street in Fig. 4 with the street name $v = 0$. It is a plot of $dx/dt|_{v=0}$ vs. x , where

$$\begin{aligned}
 dx/dt|_{v=0} = f(x, 0) = & 33 - x + |x - 6| \\
 & - |x - 12| + |x - 20| \\
 & - |x - 30| + |x - 42| - |x - 56|. \quad (5)
 \end{aligned}$$

Figure 5 shows that every intersection between the POP and x -axis, where $dx/dt = 0$, is an equilibrium point of the CCM Circuit 1 with $E = 0$. The four equilibrium points $Q_1, Q_3, Q_5,$ and Q_7 are asymptotically stable, whereas the three equilibrium points $Q_2, Q_4,$ and Q_6 are unstable, since the state variable $x(t)$ diverges away from $Q_2, Q_4,$ and Q_6 . Any initial point $x(0) > X_Q + \delta x$, where $X_Q \in \{X_{Q2}, X_{Q4}, X_{Q6}\}$ and $dx/dt > 0$, located near an unstable equilibrium points $Q_2, Q_4,$ and Q_6 must converge to an adjacent stable equilibrium points $Q_3, Q_5,$ and Q_7 on its right, as indicated by purple arrowheads in Fig. 5. Conversely, any initial point $x(0) < X_Q - \delta x$, where $dx/dt < 0$, near the unstable equilibrium points $Q_2, Q_4,$ and Q_6 must converge to an adjacent stable equilibrium points $Q_1, Q_3,$ and Q_5 on its left, as indicated by black arrowheads in Fig. 5. Moreover, the calculated eigenvalues of the stable equilibrium points are found to be *negative*, whereas the calculated eigenvalues of the unstable equilibrium points are found to be *positive*, as predicted by theory in [19, 20].

Fig. 4 Dynamic route map (DRM) of the CCM. Each curve is analogous to a street whose street name is the value of the parameter v and whose direction is indicated by an arrowhead, which follows the traffic rule: move right (resp., move left) if the street is located above (resp., below) the horizontal axis $x = 0$



2.3 Explicit parametric equations of DC V - I curve of the CCM

In circuit theory, the DC V - I curve of a two-terminal electronic device is defined as the set of all measurable or calculated points (V, I) upon application of a DC voltage V , DC current I , across the device. In general, the DC V - I curves of commercial two-terminal nonlinear resistive, or memristive, devices are generally described by a *loci* of points in the I vs. V plane because no analytical equations exist that would reproduce the measured loci of points. Moreover, for devices exhibiting strong nonlinearities, the DC V - I curve usually consist of two or more *disconnected* branches. As an example, consider the memristor [16] described by *Ohm's Law*

$$v = R(x, i) i = (0.01 x^2 i^2) i, \tag{6}$$

State Equation

$$dx/dt = f(x, i) = -x^3 - 2x^2 + (3 + i^2)x. \tag{7}$$

Equating (7) to zero, with constant (DC) current $i = I$, and solving for x , we obtain the exact equation of the following three equilibrium points

$$\text{Equilibrium Point 1: } x = X_0 = 0, \tag{8a}$$

$$\text{Equilibrium Point 2: } x = X_1 = -1 + \sqrt{4 + I^2}, \tag{8b}$$

and

$$\text{Equilibrium Point 3: } x = X_2 = -1 - \sqrt{4 + I^2}. \tag{8c}$$

Substituting Eqs. 8(a), (b), and (c) into the state-dependent Ohm's law (6), we obtain the following three *disconnected* branches of the DC V - I curve of the above memristor:

$$\text{DC } V\text{-}I \text{ Curve Branch 1 : } V = 0, \tag{9a}$$

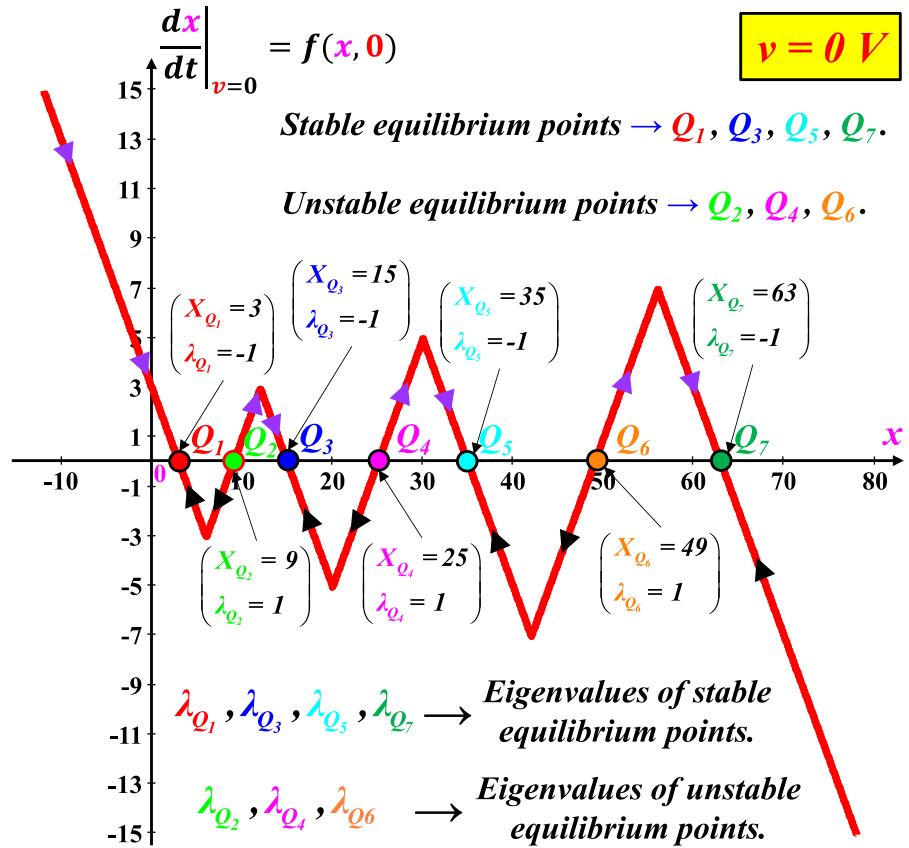
$$\text{DC } V\text{-}I \text{ Curve Branch 2 : } V = 0.01 \left[-1 + \sqrt{4 + I^2} \right] I^3, \tag{9b}$$

$$\text{DC } V\text{-}I \text{ Curve Branch 3 : } V = 0.01 \left[-1 - \sqrt{4 + I^2} \right] I^3. \tag{9c}$$

Thus, the DC V - I curve of the above memristor consists of three *separated* branches, as shown in Fig. 6.

We will now derive the *exact* analytical equation defining the DC V - I curve of the CCM defined in Fig. 1. In particular, we will derive two formulas which

Fig. 5 Power-off plot (POP) of the CCM



together gives the exact parametric equations of the DC V - I curves, with the equilibrium state $x = X$ ($-\infty < X < \infty$), as an independent parameter.

Let us assume that for each DC voltage $v = V$, the CCM has at least one equilibrium state $x = X$, namely $dx/dt|_{(v=V, x=X)} = 0$. In particular, substituting $v = V$, $x = X$, and $dx/dt = 0$ in (3), and solving for V , we obtain

$$V = - \begin{bmatrix} 33 - X + |X - 6| - |X - 12| + |X - 20| \\ -|X - 30| + |X - 42| - |X - 56| \end{bmatrix} \triangleq \hat{v}(X). \tag{10a}$$

The plot of $V = \hat{v}(X)$ in the V vs. X plane is shown in Fig. 7a. Next, substituting (10a) into (1), with $v = V$, $i = I$, and $x = X$, we obtain

$$I = -X^2 \begin{bmatrix} 33 - X + |X - 6| - |X - 12| + |X - 20| \\ -|X - 30| + |X - 42| - |X - 56| \end{bmatrix} \triangleq \hat{i}(X). \tag{10b}$$

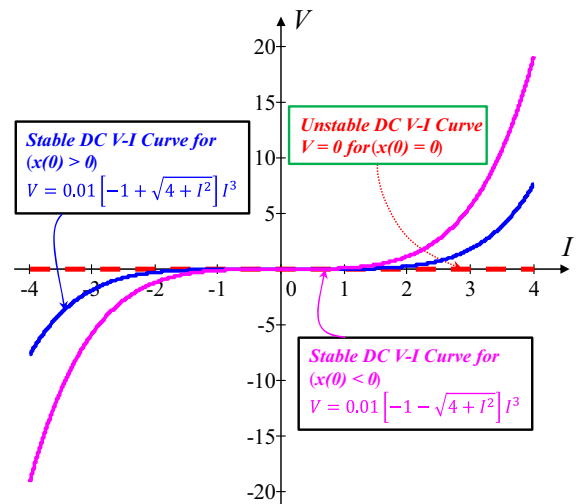


Fig. 6 A memristor and its DC V - I curve, which consists of three disconnected branches described by the unstable branch $V = 0$ (dotted red loci), and two asymptotically stable branches (for each fixed value of I) defined analytically by a blue equation for $x(0) > 0$, and by a magenta equation for $x(0) < 0$ [16]

Table 2 Coordinates of (V, I) for a sample set of X calculated from the two parametric equations, $V = \hat{v}(x)$ and $I = \hat{i}(x)$ in (10a) and (10b)

X	$V = \hat{v}(X), \text{V}$	$I = \hat{i}(X), \text{kA}$	X	$V = \hat{v}(X), \text{V}$	$I = \hat{i}(X), \text{kA}$
-12	-15	-2.16	30	-5	-4.5
-10	-13	-1.3	35	0	0
-7	-10	-0.49	40	5	8
0	-3	0	42	7	12.35
3	0	0	49	0	0
6	3	0.11	50	-1	-2.5
9	0	0	56	-7	-21.95
10	-1	-0.1	60	-3	-10.8
12	-3	-0.43	63	0	0
15	0	0	70	7	34.3
20	5	2	73	10	53.29
25	0	0	78	15	91.26

The plot of $I = \hat{i}(X)$ in the I vs. X plane is shown in Fig. 7b.

Note that the equilibrium state X in Fig. 7a, b spans the entire horizontal axis, namely $-\infty < X < \infty$. Observe that for any value $X \in (-\infty, \infty)$, we can calculate the corresponding DC voltage V , and DC current I using the *exact* formulas (10a) and (10b), respectively. Table 2 shows the values of V and I for $-12 < X < 78$, which covers the region shown in Fig. 7.

Plotting the points (V, I) from Table 2 for $-7 < X < 73$, we obtain the DC V - I curve of the *CCM* (defined in Fig. 1) shown in Fig. 7c. Observe that unlike the examples shown in Fig. 6, this DC V - I curve is a *contiguous* curve. Each point on this curve corresponds to an *equilibrium state* X , which may be *stable* (solid line) or *unstable* (dotted line).

Moreover, substituting the value of the state variable $x = X_{Q_i}$ into (10a) at the seven equilibrium states Q_i identified in Fig. 5, where $i = 1, 2, \dots, 7$, we obtain $V(X_{Q_i}) = 0$, at each of the seven equilibrium points Q_i (listed in the upper left box in Fig. 7c). It follows from the state-dependent Ohm's law in (10b) that $I(X_{Q_i}) = 0$ at all seven equilibrium states. In other words, in the DC V - I plane in Fig. 7c, the loci of the state variable x pass through the origin $(V, I) = (0, 0)$ 7 times.

It is important to observe that the DC V - I curve in Fig. 7c is obtained without solving any algebraic, or differential equations! Indeed, it is obtained by substi-

tuting any desired value of X , where $-\infty < X < \infty$, into the *explicit analytical* Eq. (10a) for $V = \hat{v}(x)$ and (10b) for $I = \hat{i}(x)$. This derivation of a memristor DC V - I curve by *direct substitution into the explicit state-dependent Ohm's law, and state equation* is a truly remarkable example for future researchers.

Observe that the inset in the lower-right corner reveals a short piece of the DC V - I curve that exhibits a *negative slope*, over $-3\text{V} < V < -1\text{V}$. This implies the Chua Corsage Memristor is *locally active* [21] and can be used to *design* an *oscillator*, which is presented in Sect. 3.

2.4 Explicit parametric equations of the fixed-point loci of *CCM*

The *fixed-point loci* of the *CCM* is defined to be the *set* of *steady-state* (constant) response of the *state variable* $x = X(V)$, calculated from the *CCM Circuit 1* in Fig. 2a upon applying a constant DC voltage $v = V$, $-\infty < V < \infty$, across the *CCM*.

Observe that the above definition assumes the *CCM* circuit in Fig. 2a is in equilibrium, namely $dx/dt|_{v=V} = 0$. The fixed-point loci of the *CCM* can be calculated by setting $dx/dt = 0$ in (3) and solving for X for each constant $v = V$; namely, the fixed-point loci of the *CCM* is the *set* of all solutions of $x = X$ of the equilibrium equation

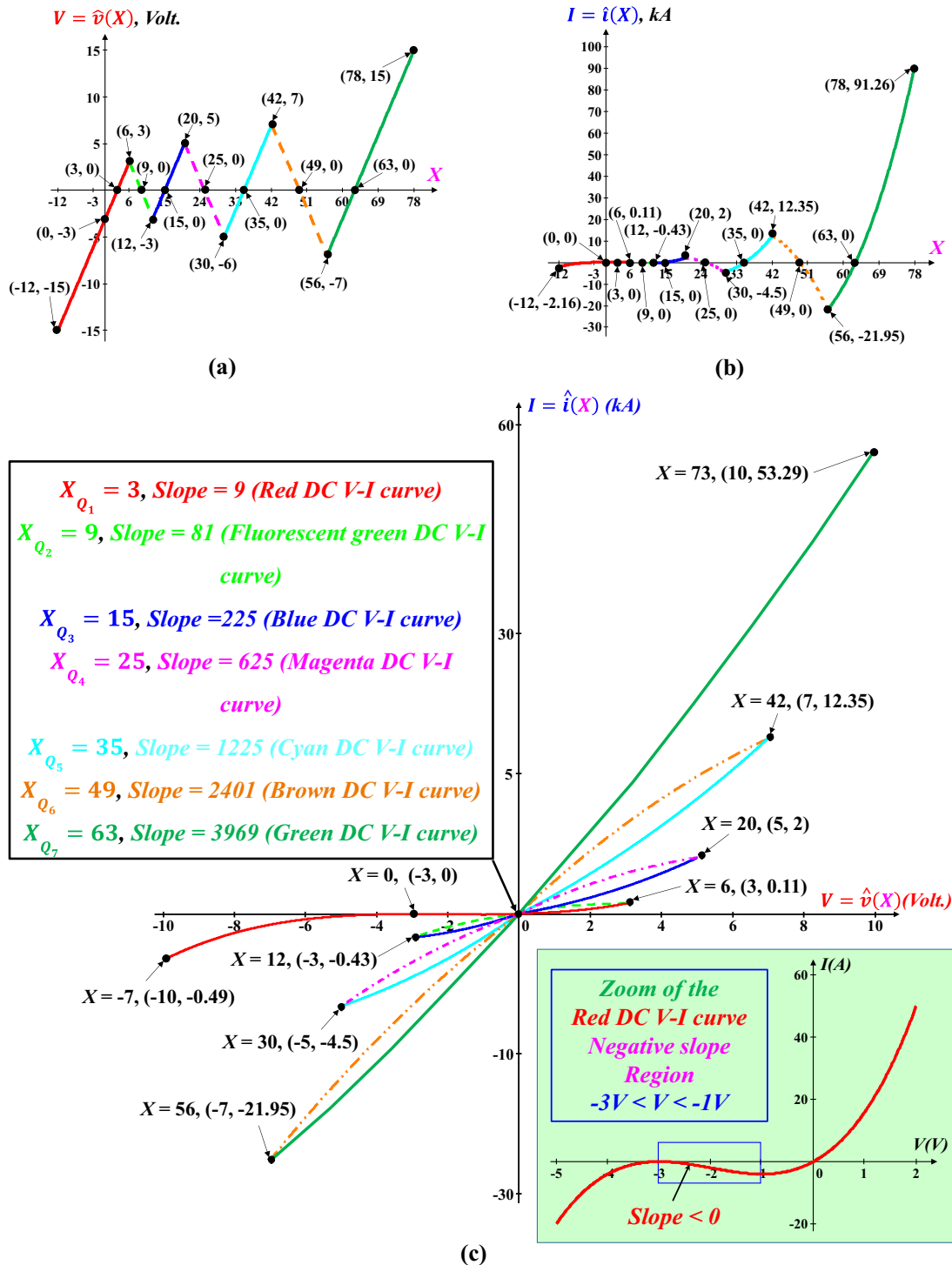


Fig. 7 Exact parametric equation of the Chua Corsage Memristor. **a** $V = \hat{v}(X)$ vs. X , and **b** $I = \hat{i}(x)$ vs. X , for each values of $\chi = \{X : -12 \leq X \leq 78\}$. **c** DC $V-I$ plot, where the coordinates (V, I) of each point are extracted from (a) and (b), for each values

of X , where $\chi = \{X : -7 \leq X \leq 73\}$. The lower-right inset shows the zoomed portion of red DC $V-I$ curve over the voltage range $-5V \leq V \leq 2V$. The upper left inset shows the state variable X values at $V = 0V$

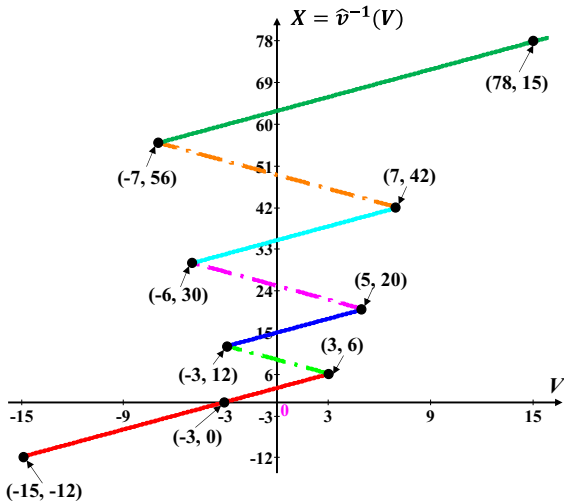


Fig. 8 Fixed-Point loci of the CCM

$$\begin{aligned}
 & f(X) + V \\
 &= \left[\begin{array}{l} 33 - X + |X - 6| - |X - 12| + |X - 20| \\ -|X - 30| + |X - 42| - |X - 56| + V \end{array} \right] \\
 &= 0.
 \end{aligned} \tag{11}$$

Using the notation in (10a), the fixed-point loci of the CCM is obtained by solving the voltage parametric equation (10a) for X, namely

$$X = \hat{v}^{-1}(V), \tag{12}$$

where $\hat{v}^{-1}(\bullet)$ denotes the inverse of the single-valued function $V = \hat{v}(X)$ given in Fig. 7a, which is obtained by replotting Fig. 7a with V as the abscissa and X as the ordinate, as shown in Fig. 8. Observe that $\hat{v}^{-1}(V)$ in (12) is a multi-valued function of V. In particular, for each V value, where $-3V < V < 3V$, X has seven fixed points. Moreover, if we substitute (12) for X in (10b), we would obtain the equation of the DC V-I curve of the CCM; namely,

$$I = \hat{i}(X) = \hat{i}(\hat{v}^{-1}(V)) \triangleq g(V). \tag{13}$$

The above equation is called a composition in mathematics and is denoted by $\hat{i} \circ \hat{v}^{-1}$. Hence, we have proved the DC V-I curve of the CCM is just the mathematical composition between the parametric equation for the current $I = \hat{i}(X)$ and the inverse voltage parametric equation $X = \hat{v}^{-1}(V)$.

2.5 Small-signal equivalent circuit model of the CCM

Small-signal device modeling is the standard nonlinear circuit analysis technique for predicting the behavior of a nonlinear device via its linearized equation about an operating point on its DC V-I curve. The small-signal equivalent circuit of the CCM is derived about an equilibrium point (V, I) , utilizing the circuit shown in Fig. 9a. Applying the Taylor series and the Laplace transform, presented in [5], the small-signal admittance function $Y(s, Q)$ of the CCM about an equilibrium point Q is obtained as,

$$Y(s, Q) \triangleq \frac{\hat{i}(s)}{\hat{v}(s)} = \frac{a_{11}(Q) b_{12}(Q)}{s - b_{11}(Q)} + a_{12}(Q) \tag{14}$$

where

$$a_{11}(Q) = v \frac{\partial G(x)}{\partial x} \Big|_Q = 2XV, \tag{15a}$$

$$a_{12}(Q) = G(x) \frac{\partial v}{\partial v} \Big|_Q = G(X)|_Q = X^2, \tag{15b}$$

$$b_{11}(Q) = \frac{\partial}{\partial x} g(x, v) \Big|_Q = -1, \tag{15c}$$

and

$$b_{12}(Q) = \frac{\partial}{\partial v} g(x, v) \Big|_Q = 1. \tag{15d}$$

The small-signal parameters of the CCM can be extracted from (14) as:

$$Y(s, V) = Y_x(s, V) + Y_y(s, V) = \frac{1}{s L_x + R_x} + \frac{1}{R_y} \tag{16a}$$

where,

$$L_x(V) = \frac{1}{a_{11}(Q) b_{12}(Q)} = \frac{1}{2XV}, \tag{16b}$$

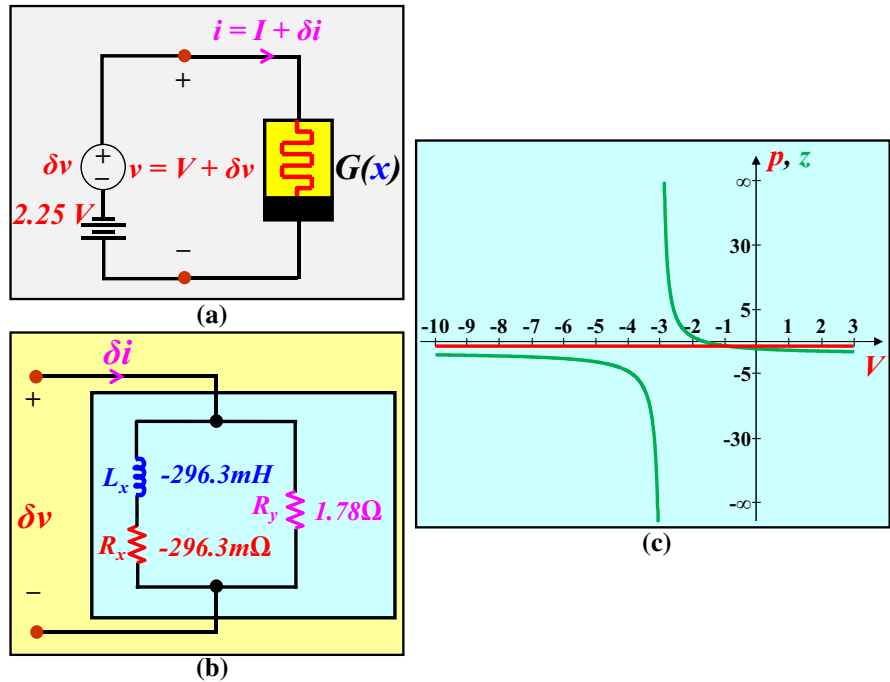
$$R_x(V) = \frac{-b_{11}(Q)}{a_{11}(Q) b_{12}(Q)} = \frac{1}{2XV}, \tag{16c}$$

and

$$R_y(V) = \frac{1}{a_{12}(Q)} = \frac{1}{X^2}. \tag{16d}$$

The small-signal equivalent circuit of the CCM computed at $V = -2.25$ V is shown in Fig. 9b. Observe that both L_x and R_x are negative, whereas R_y is positive.

Fig. 9 **a** Chua Corsage Memristor driven by $v = V + \delta v$, where $V = -2.25$ V. **b** Small-signal equivalent circuit of the CCM at $V = -2.25$ V. **c** Pole-zero diagram of the admittance function $Y(s, V)$ of the CCM over the range -10 V $\leq V \leq 3$ V



The pole $s = p$ and the zero $s = z$ of the small-signal admittance $Y(s, V)$ of the CCM Circuit 1, shown in Fig. 9c, can be obtained from (14) as :

$$Y(s, V) = \frac{a_{12}(Q)s + (a_{11}(Q)b_{12}(Q) - a_{12}(Q)b_{11}(Q))}{s - b_{11}(Q)} = \frac{b_1(V)s + b_0(V)}{a_1(V)s + a_0(V)} = \frac{K(s - z)}{(s - p)}, \tag{17a}$$

where

$$K = \frac{b_1(V)}{a_1(V)} = a_{12}(Q), \tag{17b}$$

$$p = -\frac{a_0(V)}{a_1(V)} = b_{11}(Q) = -1, \tag{17c}$$

$$z = -\frac{b_0(V)}{b_1(V)} = -\frac{[a_{11}(Q)b_{12}(Q) - a_{12}(Q)b_{11}(Q)]}{a_{12}(Q)} = -\frac{[2XV + X^2]}{X^2}. \tag{17d}$$

Observe from Fig. 9c that the pole p is constant ($\text{Re}[p] = -1$), whereas the zero z varies as a function of voltage, V .

It is well known that in order for a linear time-invariant circuit to oscillate, its admittance must have at least two poles. Hence, in order to design an oscillator using the locally active CCM, it is necessary to add at least one positive capacitor, or one positive inductor, to the CCM Circuit 1. This additional energy storage element can force the poles of the composite admittance

$Y_C(s, V)$ of the CCM to move and cross the imaginary axis of the complex plane [5,6]. The type and value of the energy storage element can be determined from the frequency response of the CCM Circuit 1. The frequency response $Y(i\omega, V)$ of the CCM at the applied DC voltage V is obtained by substituting $s = i\omega$ in (17a):

$$Y(i\omega, V) = \frac{a_0(V)b_0(V) + \omega^2 a_1(V)b_1(V)}{a_0^2(V) + \omega^2 a_1^2(V)} + i \frac{\omega (a_0(V)b_1(V) - a_1(V)b_0(V))}{a_0^2(V) + \omega^2 a_1^2(V)}, \tag{18a}$$

where

$$\text{Re } Y(i\omega, V) = \frac{a_0(V)b_0(V) + \omega^2 a_1(V)b_1(V)}{a_0^2(V) + \omega^2 a_1^2(V)} = \frac{(2XV + X^2) + \omega^2 X^2}{1 + \omega^2}, \tag{18b}$$

$$\text{Im } Y(i\omega, V) = \frac{\omega (a_0(V)b_1(V) - a_1(V)b_0(V))}{a_0^2(V) + \omega^2 a_1^2(V)} = \frac{\omega [X^2 - (2XV + X^2)]}{1 + \omega^2}. \tag{18c}$$

The frequency responses $\text{Re}[Y(i\omega, V)]$ of the CCM, parameterized by the input voltage V , at the equilibrium points Q_1, Q_3, Q_5 , and Q_7 over the frequency range -10 rad/s $\leq \omega \leq 10$ rad/s are shown

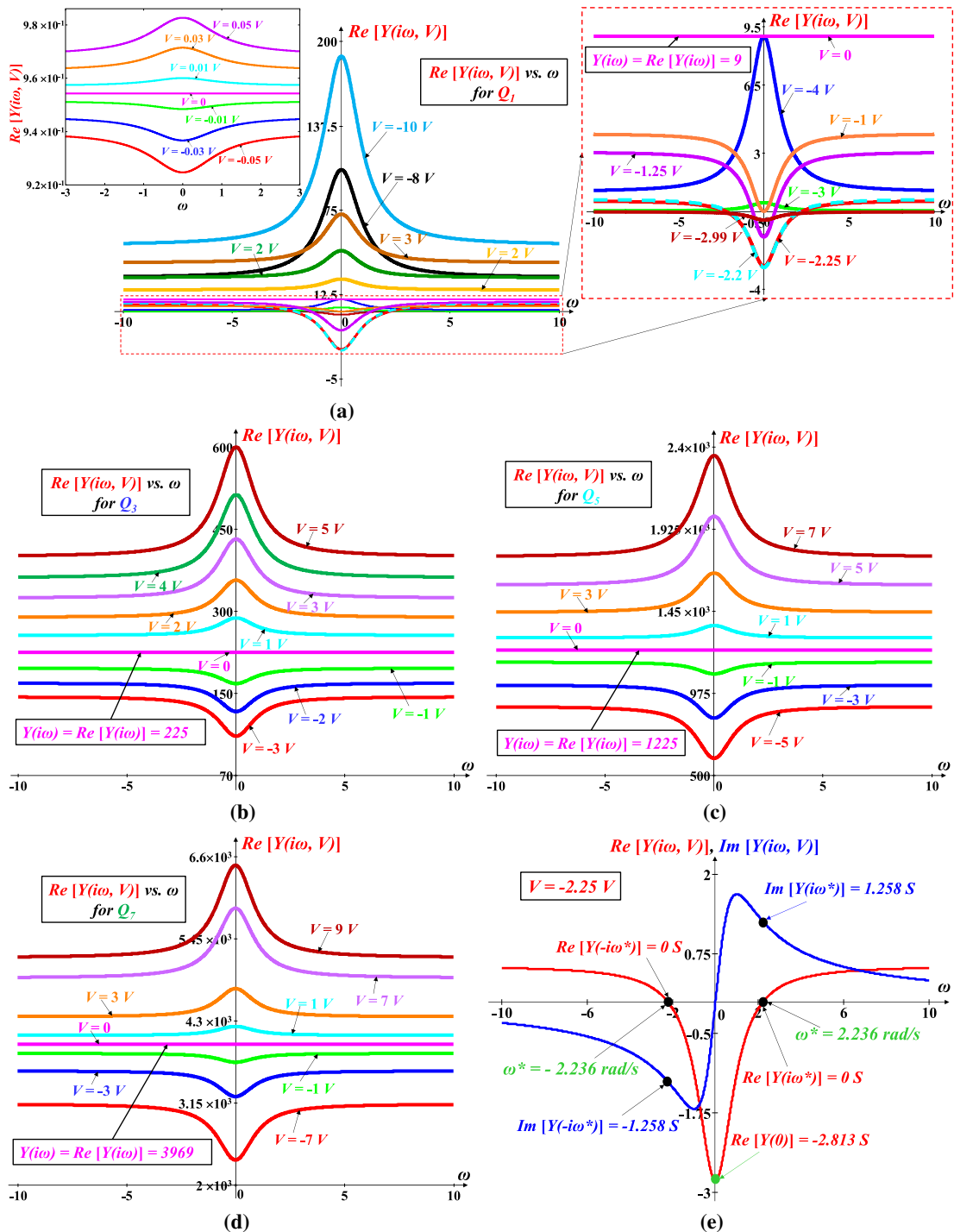


Fig. 10 Frequency response of the admittance function $Y(i\omega, V)$ of the CCM parameterized by the input voltage V . **a** $Re[Y(i\omega, V)]$ vs. ω for equilibrium point Q_1 . The left inset shows the logarithmic plot of $Re[Y(i\omega, V)]$ over the input voltage $V \in (-0.05\text{ V}, 0.05\text{ V})$, and the right inset shows the zoomed-in view near the origin of (a). **b** $Re[Y(i\omega, V)]$ vs. ω for equilibrium point Q_3 , **c** $Re[Y(i\omega, V)]$ vs. ω for equilibrium point Q_5 , **d** $Re[Y(i\omega, V)]$ vs. ω for equilibrium point Q_7 . **e** Frequency response $[Re[Y(i\omega, V)] + i Im[Y(i\omega, V)]]$ of the admittance function $Y(i\omega, V)$ of the CCM at $V = -2.25\text{ V}$ (for Q_1) over the frequency range $-10\text{ rad/s} \leq \omega \leq 10\text{ rad/s}$

librium point Q_2 , **c** $Re[Y(i\omega, V)]$ vs. ω for equilibrium point Q_5 , **d** $Re[Y(i\omega, V)]$ vs. ω for equilibrium point Q_7 . **e** Frequency response $[Re[Y(i\omega, V)] + i Im[Y(i\omega, V)]]$ of the admittance function $Y(i\omega, V)$ of the CCM at $V = -2.25\text{ V}$ (for Q_1) over the frequency range $-10\text{ rad/s} \leq \omega \leq 10\text{ rad/s}$

in Fig. 10a–d, respectively. Observe from Fig. 10a–d that $\text{Re}[Y(i\omega, V)]$ is constant for all values of ω at $V = 0$, i.e., $\text{Re}[Y(i\omega, V)]$ is independent of ω . At $V = 0$, the inductance L_x and the resistance R_x of the small-signal equivalent circuit in Fig. 9b tend to infinity, i.e., $Y_x(s, V) = 1/(sL_x + R_x) \rightarrow 0$ [see Eq. (16a)] and the corresponding impedance $Z_x(s, V) = 1/Y_x(s, V) \rightarrow \infty$ (open circuit). Hence, the admittance $Y(s, V) = Y_y(s, V) = X^2$, where the state variable X depends on the input voltage V at the equilibrium point Q_n , i.e., $X = F(V, X_{Q_n})$ where $n \in \{1, 3, 5, 7\}$. For example, the frequency response $Y(i\omega, V)$ at $V = 0$ is equal to a constant $Y(i\omega, 0)|_{Q_1} = \text{Re}[Y(i\omega, 0)]|_{Q_1} = X_{Q_1}^2 = 9$ (see Fig. 7) over the frequency range $-10 \text{ rad/s} \leq \omega \leq 10 \text{ rad/s}$, as shown in the right inset of Fig. 10a. Similarly, Fig. 10b–d shows that the frequency response $Y(i\omega, 0)|_{Q_n} = \text{Re}[Y(i\omega, 0)]|_{Q_n} = X_{Q_n}^2$, at $V = 0$, depends only on the value of the state variable X_{Q_n} listed in Fig. 7, for $n = [3, 5, 7]$, despite the frequency(ω) variation over the range $\omega \in (-\infty, \infty)$. The curve of $\text{Re}[Y(i\omega, V)]$ shown in the left inset (with logarithmic scale in $\text{Re}[Y(i\omega, V)]$) of Fig. 10a affirms that for *nonzero* voltage ($V \neq 0$) $\text{Re}[Y(i\omega, V)]$ is varying as a function of ω over the range $-3 \text{ rad/s} \leq \omega \leq 3 \text{ rad/s}$, whereas $\text{Re}[Y(i\omega, V)]$ is constant at $V = 0$. Moreover, at $V = 0$, the value of $\text{Re}[Y(i\omega, V)]$ at the equilibrium points Q_1, Q_3, Q_5 , and Q_7 , shown in Fig. 10a–d, is equal to the corresponding slopes of the DC V – I curve shown in Fig. 7.

The frequency response $Y(i\omega, V)$ of the *CCM* calculated at $V = -2.25 \text{ V}$ (for Q_1) is shown in Fig. 10e over the range $-10 \text{ rad/s} \leq \omega \leq 10 \text{ rad/s}$. Figure 10e shows that the real and imaginary parts of the frequency response $Y(i\omega)$ at $V = -2.25 \text{ V}$ are equal to $\text{Re}[Y(i\omega^*)] = 0$ and $\text{Im}[Y(i\omega^*)] = \pm 1.258S$, respectively, at $\omega^* = \pm 2.236 \text{ rad/s}$. Since $\text{Re}[Y(i\omega^*)] = 0$ and $\text{Im}[Y(i\omega^*)] \neq 0$, the *CCM* requires a *positive* inductance with value $L = L^*H$ to be connected in series with the *CCM* in Fig. 9a to satisfy the main condition for oscillation to emerge; namely, the small-signal impedance must be *zero* at $V = -2.25 \text{ V}$ [5]. The value of the inductance L^* is calculated from the following Chua oscillation formula:

$$L^* = \frac{1}{\omega^* \text{Im} Y(i\omega^*)} = 355.5 \text{ mH}. \tag{19}$$

Figure 10e shows that at $\omega = 0$ the admittance $Y(i\omega) = -2.813 S$ at $V = -2.25 \text{ V}$. This admittance is equal to the admittance of the small-signal equivalent circuit of the *CCM*, shown in Fig. 9b, but with the inductor L_x replaced by a short circuit because the impedance of an inductor at DC ($\omega = 0$) is equal to zero. In particular, $Y(0) = \left[\frac{1}{R_x} + \frac{1}{R_y} \right] = \left[\frac{-1}{296.3 \times 10^{-3}} + \frac{1}{1.78} \right] = -2.813S$.

3 Chua Corsage Memristor (CCM) oscillator circuit

The composite one-port oscillator circuit, as shown in Fig. 11a, is designed based on the *CCM Circuit 2* with an external inductance value ($L = L^* = 355.5 \text{ mH}$) and a battery ($E = -V = 2.25 \text{ V}$) connected in series with the *CCM*, where the input port current, $i = i_L = i_M$, input voltage $v = v_L + v_M$, and the memristor voltage $v_M = i_M/G(x)$. The state-dependent Ohm’s law of the *CCM* and the two nonlinear differential equations of the *Chua Corsage Memristor oscillator (CCM oscillator) circuit*⁴ are defined as follows:

State-Dependent Ohm’s Law of CCM

$$i_M = G(x) v_M. \tag{20}$$

Second-order autonomous differential equations of CCM oscillator circuit

$$\begin{aligned} dx/dt = & \left[\begin{array}{l} 33 - x + |x - 6| - |x - 12| + |x - 20| \\ - |x - 30| + |x - 42| - |x - 56| + i_L/x^2 \end{array} \right] \\ \triangleq & f(x, i_L), \end{aligned} \tag{21a}$$

$$di_L/dt = 1/L^* (V - i_L/x^2) \triangleq g(x, i_L). \tag{21b}$$

A typical trajectory of (21a)–(21b) starting from initial state $(x(0), i_L(0)) = (0.84, -1.767)$ is shown in Fig. 11b converging to a *limit cycle*. The corresponding periodic waveforms $(x(t), i_L(t))$ are shown in Fig. 11c, d, respectively.

⁴ The *CCM oscillator circuit* in Fig. 11a is a *circuit*, unlike an isolated *Chua Corsage Memristor (CCM)* which is a *two-terminal device* with two *isolated* external terminals which is not attached to any circuit. It is important to remember a *circuit* does not have dangling circuit elements with only one of its two terminals connected to the circuit, leaving other terminal dangling freely, thereby resulting in zero circuit current flowing into the element. In this case, the dangling element can be deleted without affecting the solutions of the circuit.

To verify the oscillation conditions, we compute the admittance⁵ $Y_C(s, Q)$ of the *composite* one-port \mathcal{N} consisting of the inductor L^* in series with the *CCM* in Fig. 11a. The small-signal admittance $Y_C(s, Q)$ of the composite one-port can be computed by adding the impedance $1/Y(s, Q)$ of the *CCM* and the impedance $1/Y_{L^*}$ of the external inductor [5]:

$$\frac{1}{Y_C(s, Q)} = \frac{1}{Y_{L^*}} + \frac{1}{Y(s, Q)}, \tag{22}$$

$$Y_C(s, V) = \frac{\hat{i}(s)}{\hat{v}(s)} = \frac{s a_{12}(Q) + (a_{11}(Q) b_{12}(Q) - a_{12}(Q) b_{11}(Q))}{s^2 a_{12}(Q) L^* + s (L^* a_{11}(Q) b_{12}(Q) - L^* a_{12}(Q) b_{11}(Q) + 1) + (-b_{11}(Q))} = \frac{b_1 s + b_0}{a_2 s^2 + a_1 s + a_0}, \tag{23a}$$

where

$$\left. \begin{aligned} a_2 &= a_{12}(Q) L^* = L^* X^2 \\ a_1 &= (L^* [a_{11}(Q) b_{12}(Q) - a_{12}(Q) b_{11}(Q)] + 1) \\ &= (L^* [2XV + X^2] + 1) \\ a_0 &= -b_{11}(Q) = 1 \end{aligned} \right\}, \tag{23b}$$

$$\left. \begin{aligned} b_1 &= a_{12}(Q) = X^2 \\ b_0 &= a_{11}(Q) b_{12}(Q) - a_{12}(Q) b_{11}(Q) = 2XV + X^2 \end{aligned} \right\}. \tag{23c}$$

The frequency response defined by $(\text{Re}[Z_C(i\omega, V)] + i \text{Im}[Z_C(i\omega, V)])$ of the *composite* impedance function $Z_C(s, V)$ of the one-port \mathcal{N} in Fig. 11a at an applied voltage $v = V$ is computed by substituting $s = i\omega$ in (23a) [6] and then taking its inverse:

$$Z_C(i\omega, V) = \frac{1}{Y_C(i\omega, V)} = \frac{a_0 b_0 + \omega^2 (a_1 b_1 - a_2 b_0)}{\underbrace{b_0^2 + b_1^2 \omega^2}_{\text{Re}[Z_C(i\omega, V)]}} + i \left[\frac{\omega (a_2 b_1 \omega^2 + a_1 b_0 - a_0 b_1)}{\underbrace{b_0^2 + b_1^2 \omega^2}_{\text{Im}[Z_C(i\omega, V)]}} \right]. \tag{24}$$

Figure 12 shows the real and imaginary part of the composite impedance function $Z_C(i\omega, V)$ at $V =$

⁵ Y_C denotes the admittance of the “composite” one-port \mathcal{N} made of inductor L^* in series with the *Chua Corsage Memristor* (*CCM*).

-2.25 V over the range $-10 \text{ rad/s} \leq \omega \leq 10 \text{ rad/s}$. Observe from Fig. 12 that $Z_C(i\omega^*, V = -2.25 \text{ V}) \rightarrow 0$ at $\omega = \omega^* = \pm 2.236 \text{ rad/s}$ which satisfies the prime condition of the *CCM* oscillator circuit; namely, the small-signal impedance of the composite one-port \mathcal{N} must be equal to zero at $v = V = -2.25 \text{ V}$. Observe that at $V = -2.25 \text{ V}$ and $\omega = 0$, the value of the composite impedance function $Z_C(i\omega, V) = -355.5 \text{ m}\Omega$, in Fig. 12, must be equal to the reciprocal of the admittance $Y(i\omega, V) = -2.813 \text{ S}$ at $\omega = 0$ in Fig. 10e,

because the impedance of the inductor L^* is *zero* Ohms at $\omega = 0$, so that $Z_C(i\omega, V) = 1/Y_C(i\omega, V) = 1/(-2.813 \text{ S}) = -355.5 \text{ m}\Omega$.

The poles $s = \{p_1, p_2\}$ and zero $s = z_1$ of the composite admittance $Y_C(s, V)$ in Fig. 11a are computed using (23a):

$$Y_C(s, V) = \frac{b_1 s + b_0}{a_2 s^2 + a_1 s + a_0} = \frac{(s - z_1)}{(s - p_1)(s - p_2)}, \tag{25a}$$

where

$$z_1 = -\frac{b_0}{b_1}, \tag{25b}$$

$$p_1 = \frac{-a_1 + \sqrt{a_1^2 - 4a_2 a_0}}{2a_2}, \tag{25c}$$

$$p_2 = \frac{-a_1 - \sqrt{a_1^2 - 4a_2 a_0}}{2a_2}. \tag{25d}$$

The loci of the *real* vs. *imaginary* parts of the poles $p_i = \text{Re}[p_i(V)] + i \text{Im}[p_i(V)]$ of the composite admittance $Y_C(s, V)$ of the composite one-port \mathcal{N} in Fig. 11a, parameterized by the input voltage V over the range $-3 \text{ V} \leq V \leq 3 \text{ V}$, are shown in Fig. 13. The arrowheads indicate the direction of the movement of the poles. Observe the *complex conjugate* poles of $Y_C(s, V)$ in Fig. 13 lie in both the left-hand side and the right-hand side of the imaginary axis. Observe also that there are two pairs of complex conjugate poles on the imaginary axis at $V = -2.25 \text{ V}$ and $V = -1.75 \text{ V}$, respectively. The inset of Fig. 13 shows

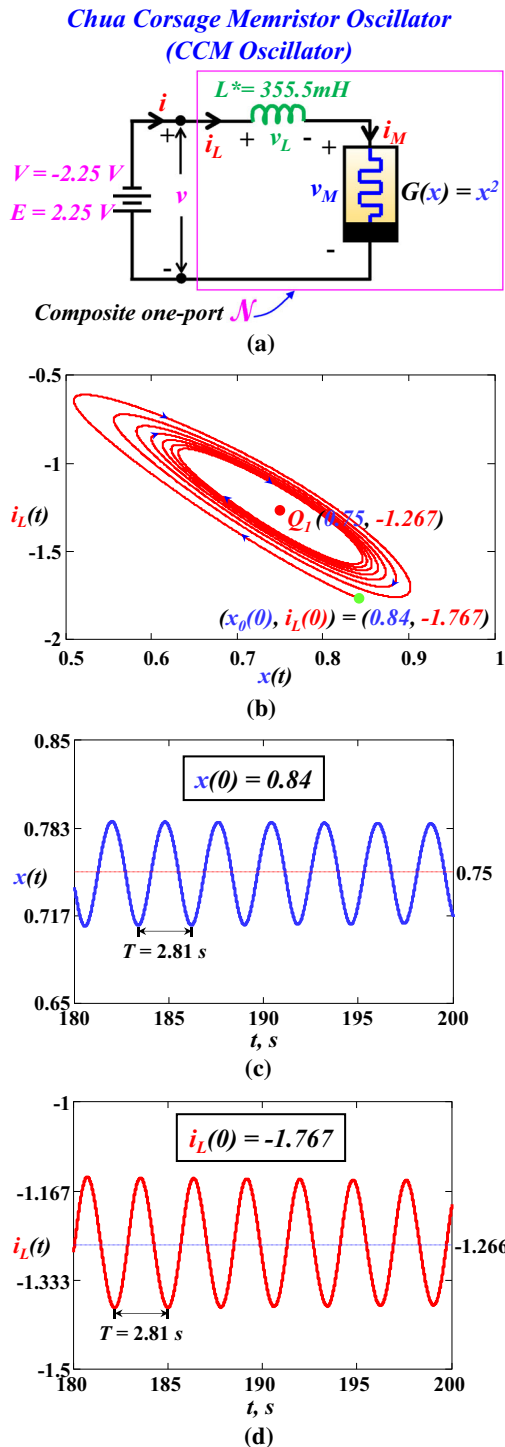


Fig. 11 Circuit diagram of CCM oscillator circuit with $E = 2.25 \text{ V}$, **b** a trajectory with initial state $(x(0), i_L(0)) = (0.84, -1.767)$ in the phase plane. **c** Periodic waveforms of $x(t)$ with $T = 2.81 \text{ s}$, and **d** corresponding periodic waveforms of $i_L(t)$

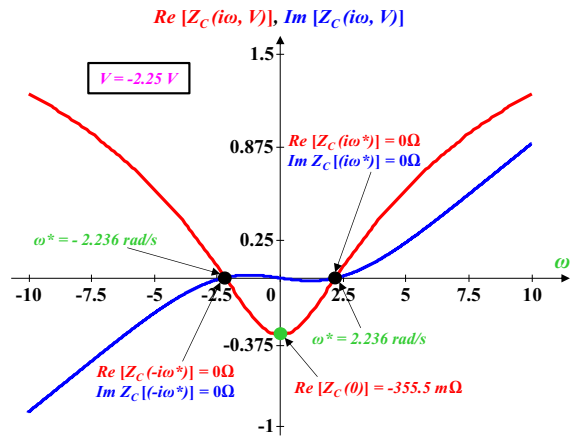


Fig. 12 Frequency response $\text{Re}[Z_C(i\omega, V)]$ and $\Im[Z_C(i\omega, V)]$ of the composite impedance function $Z_C(i\omega, V)$, plotted as a function of frequency ω , with $V = -2.25 \text{ V}$ and $L = L^* = 355.5 \text{ mH}$

that $\text{Re}[p_1] > 0$ and $\text{Re}[p_2] > 0$ for input voltages $-2.25 \text{ V} < V < -1.75 \text{ V}$.

Figure 14 shows the loci of the $\text{Im}[p_1]$ and $\text{Im}[p_2]$ of the poles vs. $\text{Re}[p_1]$ and $\text{Re}[p_2]$ of the poles p_1 and p_2 of $Y_C(s, V)$, parameterized by the value of inductance L at DC input voltage $V = -2.25 \text{ V}$, where the arrowheads indicate the direction of movement of the poles. The pole diagram in Fig. 14 contains a pair of complex conjugate poles located at $\text{Im}[p_1] = 2.236$ and $\text{Im}[p_2] = -2.236$ at the inductance value of $L = L^* = 355.5 \text{ mH}$. Observe also when the inductance $L \rightarrow 0$, $\text{Re}[p_1] \rightarrow -1$ and $\text{Re}[p_2] \rightarrow -\infty$ and when $L \rightarrow \infty$, $\text{Re}[p_1] \rightarrow 5$ and $\text{Re}[p_2] \rightarrow 0$, respectively.

Figure 13 shows that the external inductance L^* in the CCM oscillator circuit compels the constant poles of CCM [shown in Fig. 9c] to cross the imaginary axis of the complex plane. The right-hand side poles and the complex conjugate poles on the imaginary axis of the complex plane, in Fig. 13, might give rise to bifurcation. Moreover, Fig. 14 shows that the complex conjugate poles ($\text{Im}[p_1] = 2.236$ and $\text{Im}[p_2] = -2.236$) on the imaginary axis for an inductance $L = L^* = 355.5 \text{ mH}$ are equal to the operating frequency $\omega = \omega^* = \pm 2.236 \text{ rad/s}$ (in Fig. 12). Thus, Figs. 13 and 14 affirm that the Hopf bifurcation points at $V = -2.25 \text{ V}$ and $V = -1.75 \text{ V}$ or a small neighborhood of these two points on the open right-half plane, in Fig. 13, might give rise to stable oscillation by exploiting the Hopf bifurcation.

Fig. 13 Loci of the real and imaginary parts of the poles p_1 and p_2 of the admittance $Y_C(s, V)$ of the composite one-port \mathcal{N} of the CCM oscillator as a function of input voltage V , where the inductance $L = L^* = 355.5 \text{ mH}$

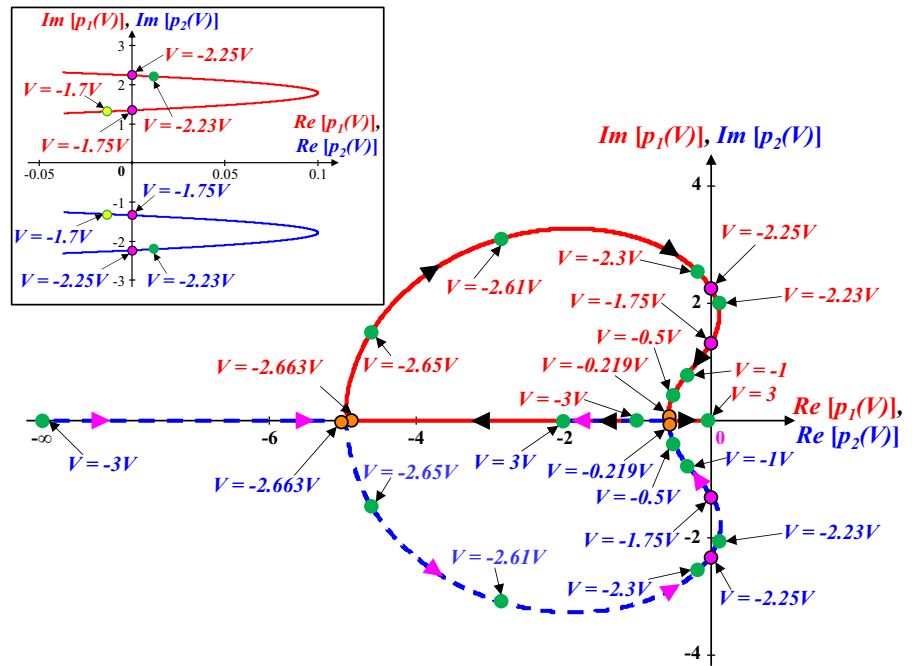
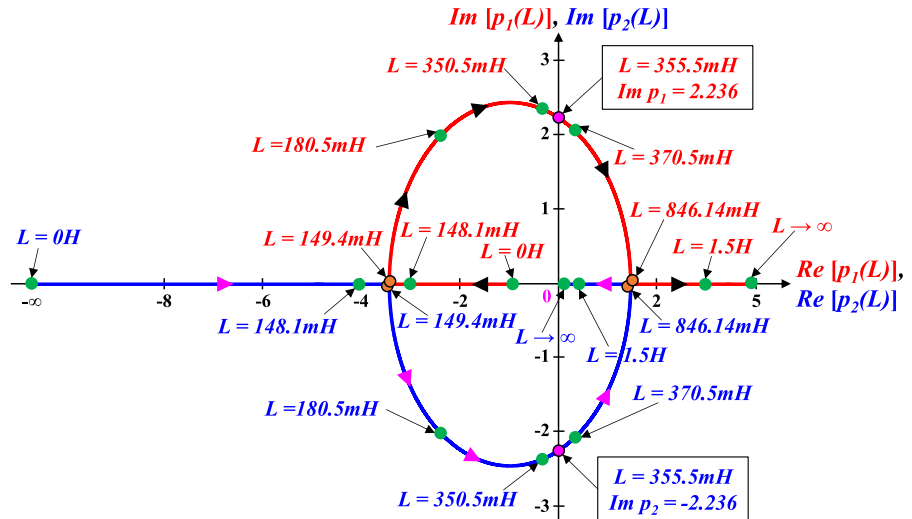


Fig. 14 Loci of the real and imaginary parts of poles of the composite admittance $Y_C(s, V)$ of the CCM oscillator, plotted as a function of the external inductance L , at the applied battery voltage $V = -2.25 \text{ V}$. To avoid clutter, we choose an uneven horizontal scaling between 2 and 5 in the horizontal axis



4 Bifurcation analysis

The presence of *complex phenomena* in a nonlinear dynamical system is predicted by the local activity principle [21]. In particular, it asserts that a nonlinear circuit made of two-terminal circuit elements, and/or more complicated two-terminal devices, or *one-ports* [22], can exhibit complex *bifurcation* phenomena, such as *oscillation* and *chaos* only if the circuit contains at least one nonlinear locally active element. There is a funda-

mental deep mathematical theorem given in [21] which allows one to test whether a two-terminal element, or *one-port*⁶, is *locally active* about some *equilibrium point*, aka a DC operating point. While a rigorous proof of this theorem is couched in abstruse mathematics, testing whether a two-terminal element, or one-port,

⁶ Any two-terminal electronic device, or an interconnection of electronic devices, enclosed by a package, aka a *black box*, with only two externally accessible conducting wires is called a *one-port* [22]. Hence, all two-terminal devices are examples of one-ports.

is locally active involves only standard sophomore-level mathematics. In particular, the test is couched in terms of the *small-signal impedance* $Z(s)$, or admittance $Y(s) \triangleq 1/Z(s)$, derived from an equilibrium point (or *DC operating point*) Q of the two-terminal element, or one-port \mathcal{N} .

4.1 Simple test for local activity

A two-terminal element or one-port \mathcal{N} is *locally active* at an equilibrium point (or a point on its associated DC V - I curve) Q if at least one of the following two criteria is satisfied:

Local Activity Criterion 1 Either $Z(s)$, or $Y(s)$, has a pole $s = p$ located in the open right-half s -plane, i.e., $\text{Re}[s] > 0$.

Local Activity Criterion 2 Either $\text{Re}[Z(i\omega)] < 0$, or $\text{Re}[Y(i\omega)] < 0$, for at least one frequency ω .

Here, $Z(s)$ (resp., $Y(s)$) denotes the small-signal *impedance* (resp., *admittance*) about Q .

Example 1 Local Activity regime of the CCM

Consider the DC V - I curve of the CCM in Fig. 7c. Observe that the *slope* at any point on the DC V - I curve over $-3V < V < -1V$ (see the enlarge inset in lower-right corner) is negative. It follows from the derivations in Sect. 2.5 that the slope at DC operating point Q is equal to the $\text{Re}[Y(i\omega)]$ calculated at Q .

Since the slope at any point Q over the interval $-3V < V < -1V$ in Fig. 7c is negative, $\text{Re}[Y(i\omega)] < 0$ at Q and $\omega = 0$. Here, $\omega = 0$ because the testing signal is a DC battery.

It follows from the Local Activity Criterion 2 that the CCM is *locally active* at any DC operating point over the range $-3V < V < -1V$.

4.2 Edge of chaos

The preceding subsection shows that there are at least two avenues for a two-terminal element, or one-port \mathcal{N} , to be locally active. Example 1 is locally active at Q because the CCM satisfies the Local Activity Criterion 2. There are other examples where a two-terminal element, or one-port, is locally active because it satisfies the Local Activity Criterion 1. In fact, there are many examples of locally active elements which satisfies *both* criterion 1 and criterion 2.

However, there exists a *much smaller* subset of *locally active* two-terminal elements, or one-ports, which satisfies only Criterion 2, in the sense that all poles p_i of its *impedance* $Z(s)$ (resp., *admittance* $Y(s)$) are located in the open left-half plane; namely, $\text{Re} p_i < 0, i = 1, 2, \dots, n$, assuming $Z(s)$ (resp., $Y(s)$) has “ n ” poles.

This relatively small subclass of *locally active impedances* $Z(s)$ (resp., *admittances* $Y(s)$) which satisfies only Local Activity Criterion 2, but *not* Criterion 1, is said to be operating in the *edge of chaos* [21].

Since there are two independent chances for an impedance $Z(s)$ (resp., admittance $Y(s)$) of a two-terminal element, or one-port, to be locally active, but *only one chance* for it to be on the *edge of chaos*, it is much harder to earn the accolade of belonging to the *edge of chaos* club.

The reason why elements belonging to the edge of chaos club are superior over those that are only locally active is the following fundamental hypothesis in [21, 23].

Complexity Hypothesis *Complex phenomena* such as power amplification, oscillation, chaos, catastrophic events, and artificial intelligence tend to emerge over parameter ranges of a device or system, operating on, or near the neighborhood of the system’s *edge of chaos* domain.

Example 2 Edge of chaos domain of the CCM

Let us derive the parameter domain where the CCM defined in Fig. 9a is operating on the *edge of chaos*.

Figure 9c shows the admittance $Y(s)$ of the CCM has only one pole $p = -1$ for $-\infty < V < \infty$. Hence, the Local Activity Criterion 1 cannot be satisfied by the admittance $Y(s, V)$ of the CCM over all DC battery voltage $-\infty < V < \infty$. However, observe from Fig. 10a that $\text{Re}[Y(i\omega, V)] < 0$ over the open interval $-3V < V < -1V$. It follows from the Local Activity Criterion 2 that an *edge of chaos domain* of the CCM exists over $-3V < V < -1V$.

4.3 Hopf bifurcation

Nonlinear dynamical systems satisfying the *edge of chaos criterion* can exhibit bifurcation from a stable equilibrium point regime to a *chaotic* regime by forced excitation [24]. In a local bifurcation, called the *Hopf*

bifurcation, an equilibrium point of the system’s differential equations loses its stability as a pair of complex conjugate eigenvalues, or equivalently poles of its associated admittance $Y(s, V)$ or impedance $Z(s, I)$ if the *CCM* is driven by a *DC voltage source* V or *current source* I , cross the imaginary axis of the complex plane at some critical parameter value μ_c [25]. The Hopf bifurcation theorem asserts that under a relatively general situation, a small-amplitude sinusoidal oscillation will emerge for the control parameter $\mu > \mu_c$, and its amplitude A increases proportional to $\sqrt{\mu - \mu_c}$, for μ close to μ_c [25,26]. The *CCM oscillator* circuit exhibits *Hopf bifurcation* as it is endowed with critical *Hopf bifurcation points*, namely two pairs of complex conjugate poles at $V = -2.25$ V and $V = -1.75$ V on the imaginary axis of the complex plane shown in Fig. 13.

The Hopf bifurcation exhibited in the *CCM oscillator circuit* is classified as *supercritical* because the typical supercritical amplitude function $A_v(V) = \sqrt{\bar{x}^2 + \bar{i}_L^2}$ (where \bar{x} and \bar{i}_L denote the amplitude of the small sinusoidal $x(t)$ and $i_L(t)$) at $V = 2.25$ V and $V = -1.75$ V shown in Fig. 15a, b as a function of V is quite similar to the curve computed from the analytical formulas⁷ $A_{m1}(V) = k_1[\sqrt{|V + 2.25|}]$ and $A_{m2}(V) = k_2[\sqrt{|V + 1.75|}]$ with control parameter $\mu = V$, critical parameter values $\mu_{c1} = -2.25$ and $\mu_{c2} = -1.75$, and constants $k_1 = 2.65$ and $k_2 = 8.75$, respectively. For further assurance of a *supercritical Hopf bifurcation*, we plotted the amplitude $A_L(L) = \sqrt{\bar{x}^2 + \bar{i}_L^2}$ of the *CCM Oscillator circuit* with the inductance L as a bifurcation parameter in Fig. 15c.

According to the supercritical Hopf bifurcation theorem [26–28], the *CCM oscillator circuit* must exhibit a small stable near-sinusoidal oscillation, i.e., a *limit cycle*, over a small range of V beyond the critical parameter value $\mu_c = V = -2.25$ V. Figure 16a, d shows that the transient waveforms converge to two asymptotically stable equilibrium points $Q_0^1(0.7, -1.127)$ for the parameter value $V = -2.3$ V [which is near but to the left of the first Hopf bifurcation point $V = -2.25$ V (see inset of Fig. 13)], and $Q_0^2(1.3, -2.873)$ for $V = -1.7$ V (which is near but to the left of the second Hopf bifurcation point

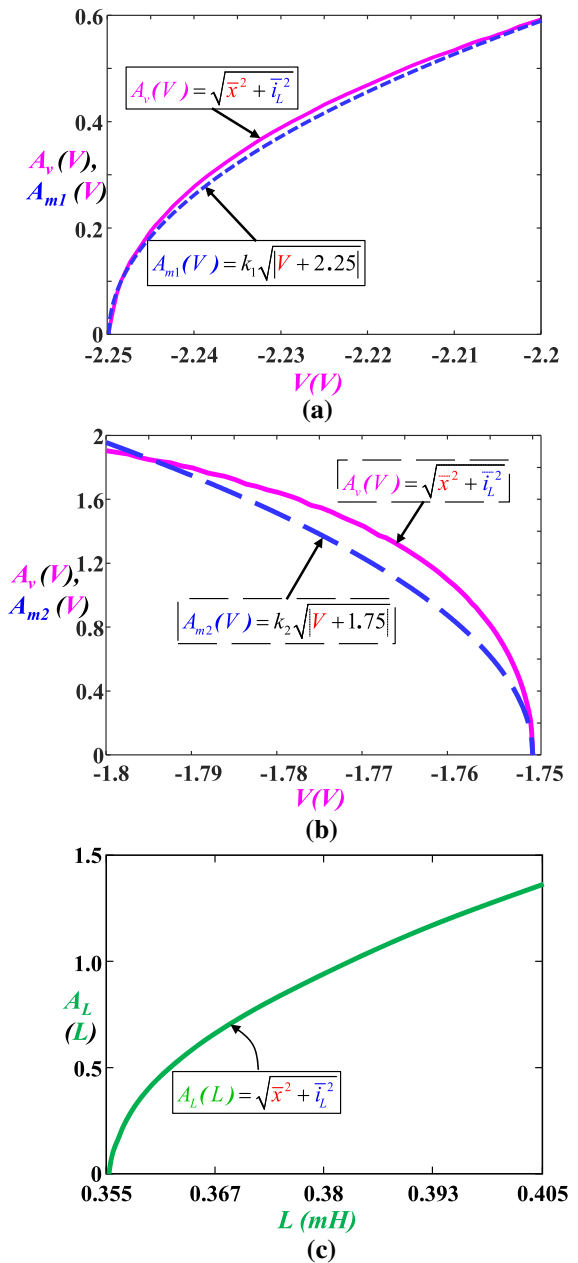


Fig. 15 Numerical verification of supercritical Hopf bifurcation of the *CCM oscillator circuit* as a parameter of V , near **a** first Hopf bifurcation point $V = -2.25$ V, and **b** second Hopf bifurcation point $V = -1.75$ V. **c** Verification of supercritical Hopf bifurcation of the *CCM oscillator* with the inductance L as the bifurcation parameter

⁷ To avoid the emergence of complex number, the absolute value of $(\mu - \mu_c)$ is used in the analytical formulas. The constants $k_1 = 2.65$ and $k_2 = 8.75$ are determined empirically.

$V = -1.75$ V), respectively. Observe, however, that the transient waveforms generated from two different initial states ($x(0) = 0.95, i_L(0) = -2.031$) and

($x(0) = 0.8, i_L(0) = -1.43$) in Fig. 16b converge to the yellow stable limit cycle for $V = -2.23$ V (which is near but to the right of the first Hopf bifurcation point $V = -2.25$ V). Moreover, transient waveforms generated from two different initial states ($x(0) = 1.1, i_L(0) = -2.431$) and ($x(0) = 1.2, i_L(0) = -3.53$) for $V = -1.77$ [which is near but to the right of the second Hopf bifurcation point $V = -1.75$ V (see inset of Fig. 13)] converge to a larger yellow limit cycle shown in Fig. 16c. The numerical simulation results shown in Fig. 16 confirm that the *CCM oscillator circuit* exhibits a stable limit cycle when the bifurcation parameter $\mu = V$ is chosen between the Hopf bifurcation points at $V = -2.25$ V and $V = -1.75$ V, as predicted by the supercritical Hopf bifurcation theorem.

In addition, the supercritical Hopf bifurcation phenomenon of the composite *CCM oscillator circuit* in Fig. 11a is also verified by choosing the external inductance L as the bifurcation parameter $\mu = L$, (with the input voltage $V = -2.25$ V) as shown in Fig. 17. Observe that for the parameter value $\mu = L = 350.5$ mH $< L^* = 355.5$ mH, the transient waveforms in Fig. 17a converge to a stable equilibrium point $Q_0(0.75, -1.27)$, whereas for $\mu = L = 356$ mH the transient waveforms converge to a *very small* stable limit cycle, as shown in Fig. 17b. Figure 17c shows that the transient waveforms generated from the two different initial states ($x(0), i_L(0) = (0.95, -2.031)$) and ($x(0), i_L(0) = (0.75, -1.27)$) converge to the green limit cycle for the parameter value $\mu = L = 370.5$ mH, where $L = 370.5$ mH $> L^* = 355.5$ mH. It follows from Fig. 17 that the *CCM oscillator circuit* exhibits a supercritical Hopf bifurcation at $\mu = L \geq L^* = 355.5$ mH resulting in a limit cycle, whereas at $\mu = L < L^* = 355.5$ mH it converges to a stable equilibrium point, as predicted by supercritical Hopf bifurcation theorem.

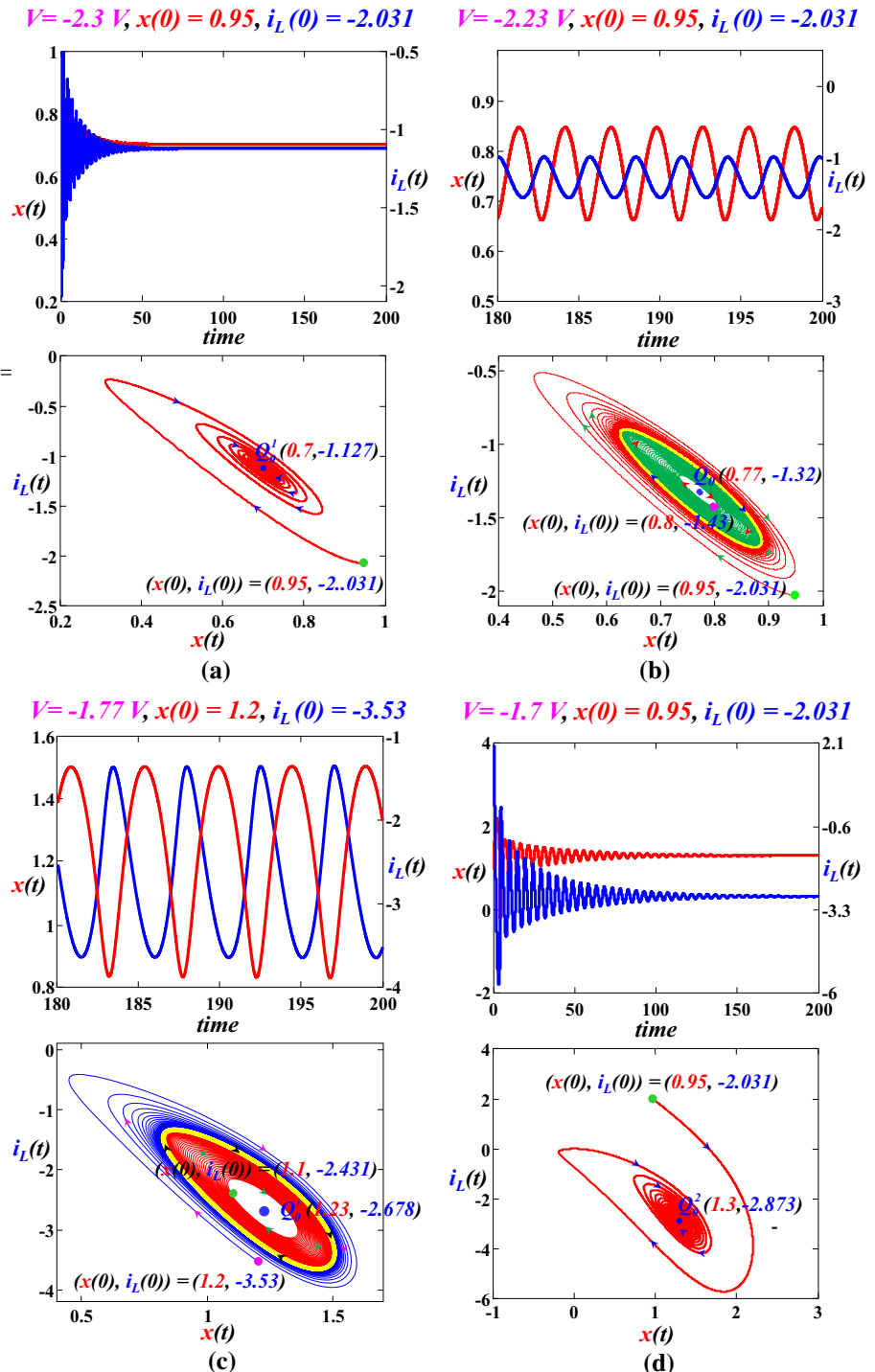
It is very interesting to observe that the numerical simulation results in Figs. 16 and 17 show that although Q_1 is *stable* in the *CCM Circuit 1*, it has become *unstable* in the composite *CCM Circuit 2*, by merely adding a *passive* circuit element, namely $L > 0$. This phenomenon is a *fundamental feature of the edge of chaos* property; namely, *it is possible to destabilize a stable circuit* (i.e., without oscillation) and make it *oscillate*, by adding only *passive* circuit elements.

5 Phase portrait

A *phase portrait* consists of a family of *trajectories* corresponding to differential initial conditions of a dynamical system in the phase plane. It is an invaluable graphical tool to visualize the qualitative behavior of the solutions of a second-order *autonomous system* of two ordinary differential equations. The phase portrait of a dynamical system reveals information about the presence of an *attractor*, a *repeller*, or a *limit cycle* for the chosen parameter values [26,29]. The stable and unstable equilibrium points in a phase portrait are called an *attractor* or *sink*, and a *repeller* or *source*, respectively. The Cartesian plane where the family of solution curves reside is called the *phase plane* and the curves traced by the solutions, with the time t as hidden parameter, are called *trajectories* [26,29]. Since every initial state of the *CCM Circuit 1* (with only one state variable x) converges to one of four stable equilibrium points (Q_1, Q_3, Q_5 , and Q_7) and diverges from three unstable equilibrium points (Q_2, Q_4 , and Q_6) at $V = 0$, one might conjecture that the phase portrait of the second-order *CCM oscillator*, based on the *CCM Circuit 2* (with two state variables x and i_L), could also exhibit *four attractors* and *three repellers* in the phase plane. But this conjecture is *false* as already shown in Figs. 16 and 17.

The phase portrait of the *CCM oscillator circuit* is shown in Fig. 18 with DC battery voltage $V = -2.23$ V and inductance $L = L^* = 355.5$ mH. In Fig. 18, the arrowheads attached to the red, blue, cyan, and green trajectories indicate the direction of motion of the composite oscillator state (x, i_L) from the initial state ($x(0), i_L(0)$) (marked in black dots). Figures 18 and 19a show that the red trajectories converge to a small *limit cycle* surrounding the unstable equilibrium point $Q_1(x_{Q1} = 0.77, i_{L_{Q1}} = -1.32)$. All blue, cyan, and green trajectories, in Figs. 18 and 19b–d, converge to the stable equilibrium points $Q_3(x_{Q3} = 12.77, i_{L_{Q3}} = -363.65)$, $Q_5(x_{Q5} = 32.77, i_{L_{Q5}} = -2394.73)$, and $Q_7(x_{Q7} = 60.77, i_{L_{Q7}} = -8235.37)$, respectively. Observe, however, the trajectories in a small neighborhood of the three unstable equilibrium points $Q_2(x_{Q2} = 11.23, i_{L_{Q2}} = -281.23)$, $Q_4(x_{Q4} = 27.23, i_{L_{Q4}} = -1653.48)$, and $Q_6(x_{Q6} = 51.23, i_{L_{Q6}} = -5852.66)$ diverge from them as shown in green dashes passing through Q_2 and Q_3 in Fig. 19e and in magenta and brown curves in Fig. 18. Each of these dash curves is called a *separatrix*. Since each tra-

Fig. 16 Numerical simulation results of the supercritical Hopf bifurcation theorem with $L = L^* = 355.5$ mH. **a** Transient waveform converges to $Q_0^1(0.7, -1.127)$ for $V = -2.3$ V with initial condition $(x(0), i_L(0)) = (0.95, -2.031)$, **b** transient waveforms generated from two different initial states $(x(0), i_L(0)) = (0.95, -2.031)$ and $(x(0), i_L(0)) = (0.8, -1.43)$ converge to a yellow limit cycle for $V = -2.23$ V, **c** transient waveforms generated from two different initial states $(x(0), i_L(0)) = (1.1, -2.431)$ and $(x(0), i_L(0)) = (1.2, -3.53)$ converge to a large yellow limit cycle for $V = -1.77$ V, and **d** transient waveform converges to $Q_0^2(1.3, -2.873)$ for $V = -1.7$ V with initial condition $(x(0), i_L(0)) = (0.95, -2.031)$



jectory can converge either to the limit cycle surrounding the unstable equilibrium point Q_1 , or to one of the three stable equilibrium points Q_3, Q_5 , and Q_7 , or can diverge from Q_2, Q_4 , and Q_6 , it follows that the phase

portrait of the CCM Circuit 2 has three attractors (Q_3, Q_5 , and Q_7) and four repellers (Q_1, Q_2, Q_4 , and Q_6). Observe that although the equilibrium point Q_1 is stable in the CCM Circuit 1, it has become unstable and

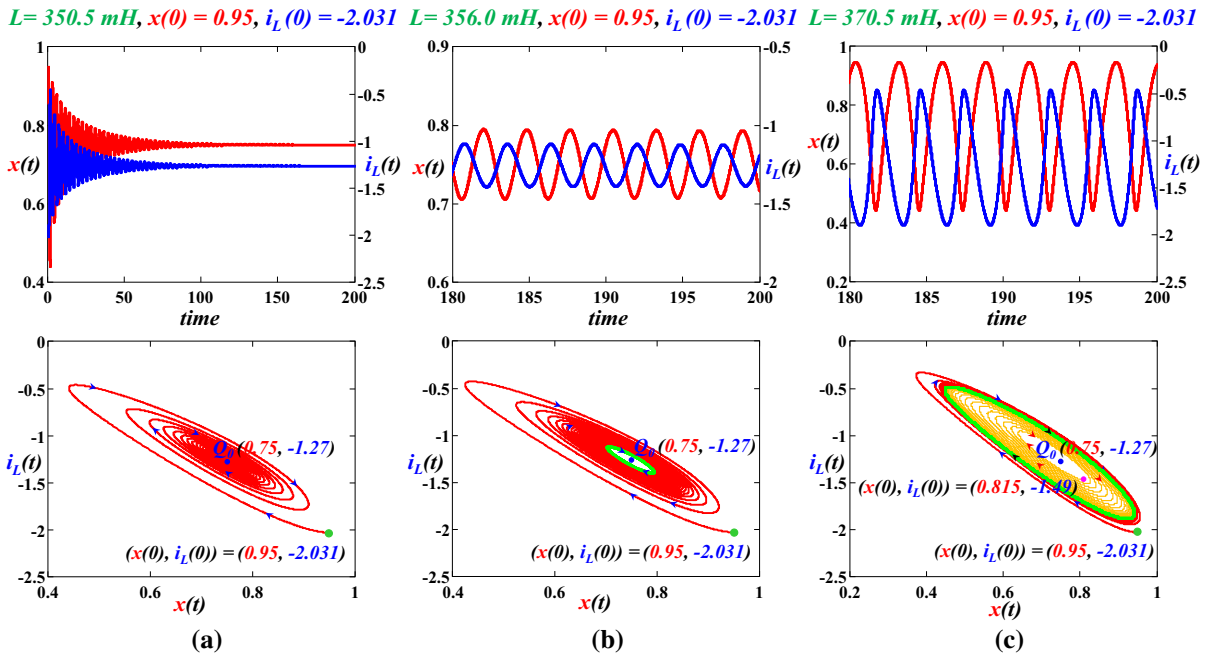


Fig. 17 Simulation results illustrating supercritical Hopf bifurcation at $V = -2.25 \text{ V}$. **a** Transient waveform from initial condition $(x(0), i_L(0)) = (0.95, -2.031)$ converges to the asymptotically stable equilibrium point $Q_0(0.75, -1.27)$ for $L = 350.5 \text{ mH}$. **b** Transient waveform from initial condition

$(x(0), i_L(0)) = (0.95, -2.031)$ converges to a stable limit cycle for $L = 356 \text{ mH}$. **c** Transient waveforms generated from two different initial states $(x(0), i_L(0)) = (0.95, -2.031)$ and $(x(0), i_L(0)) = (0.75, -1.27)$ converge to a relatively large green limit cycle for $L = 370.5 \text{ mH}$

diverges from Q_1 while converging to a limit cycle in the composite *CCM Circuit 2* when $V = -2.23 \text{ V}$, as shown in Figs. 16b and 19a.

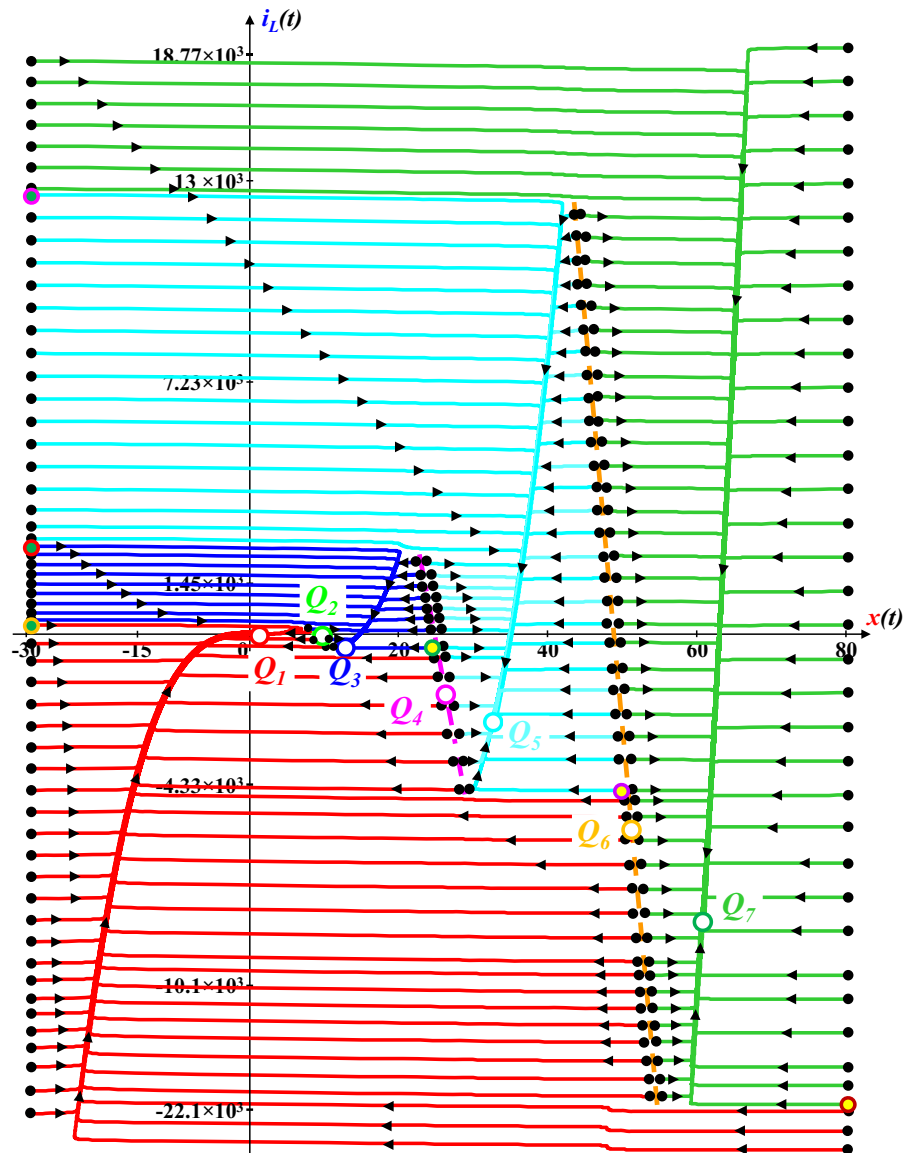
Observe from Fig. 19e that all the trajectories starting from initial states to the left of the Q_2 separatrix converge to a small *stable limit cycle* surrounding repeller Q_1 , whereas trajectories starting from initial states to the right of the Q_2 separatrix converge to the stable equilibrium point Q_3 . The region on the left side of the Q_2 separatrix is called the *basin of attraction* of the stable limit cycle, and the region on the right side of the Q_2 separatrix is called the *basin of attraction* of the stable equilibrium point Q_3 . Similarly, trajectories starting from any initial state to the left of the Q_4 separatrix converge to either the *basin of attraction* of the stable equilibrium point Q_3 or to the *basin of attraction* of the stable limit cycle, as shown in Fig. 18. In contrast, trajectories starting from initial states to the right of the Q_4 separatrix belong to the *basin of attraction* of the stable equilibrium point Q_5 and would converge to Q_5 , as shown in Fig. 18. Similar dynamics also hap-

pens for initial states starting from either sides of the Q_6 separatrix, as shown in Fig. 18.

6 Basins of attractions of coexisting pinched hysteresis loops

The steady-state dynamics of a memristor or memristive system depends on the initial condition of the state variables. Under a periodic bipolar excitation, a memristor circuit can exhibit different asymptotic behaviors for different initial states [30, 31]. For such systems, the state space contains multiple attractors where each one has its own basin of attraction. A state-space trajectory would converge to an attractor whose basin of attraction contains the initial state $x(0)$ [26]. The steady-state behavior of the dynamic attractors of the *CCM Circuit 3*, driven by a sinusoidal excitation $v_s(t) = A \sin(\omega t)$, where $\omega = 2\pi f$, with different amplitudes A , frequencies f , and initial states $x(0)$ is shown in Figs. 20 and 21. For simplicity, let us fix the amplitude A of the input voltage and consider four frequencies $\{f_1,$

Fig. 18 Phase portrait of the CCM oscillator circuit for DC battery voltage $V = -2.23$ V with external inductor $L = L^* = 355.5$ mH. The separatrix emerging from the unstable equilibrium points Q_4 and Q_6 is drawn as magenta and brown dashes loci, respectively

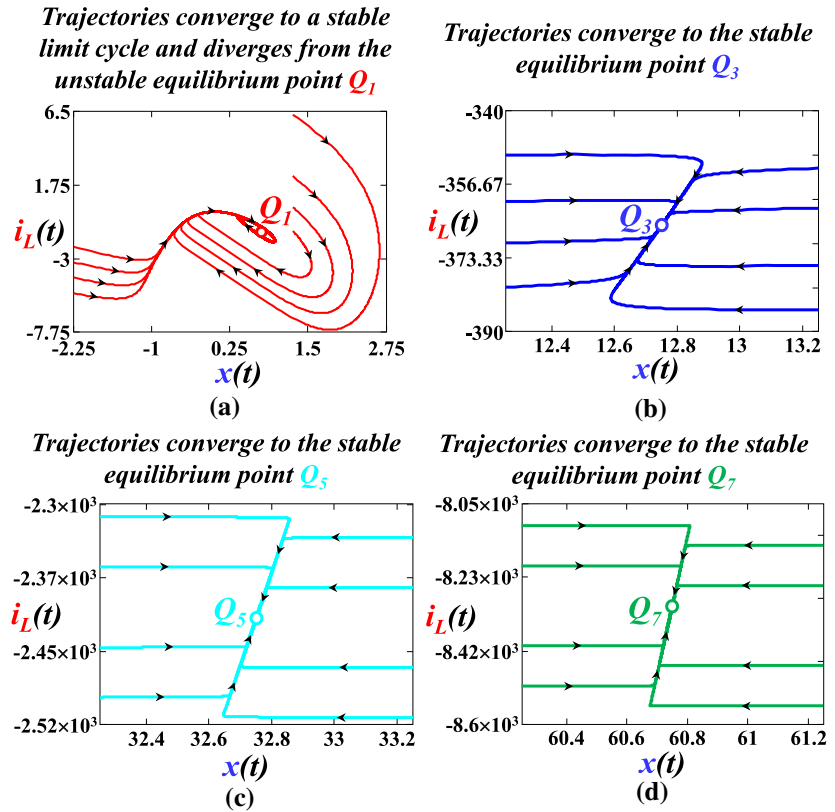


$f_2, f_3, f_4 = \{0.01, 0.1, 0.5, 1\}$ Hz. For amplitude $A = 1$ V and $A = 3$ V of the sinusoidal excitation, the corresponding four distinct *stable* periodic steady-state responses $x_j(t)$ of the CCM Circuit 3 are shown in Figs. 20 and 21, respectively. The corresponding basins of attraction $B_j(0)$ of the $x_j(t)$, $j \in \{a, b, c, d\}$, are listed in their corresponding insets.

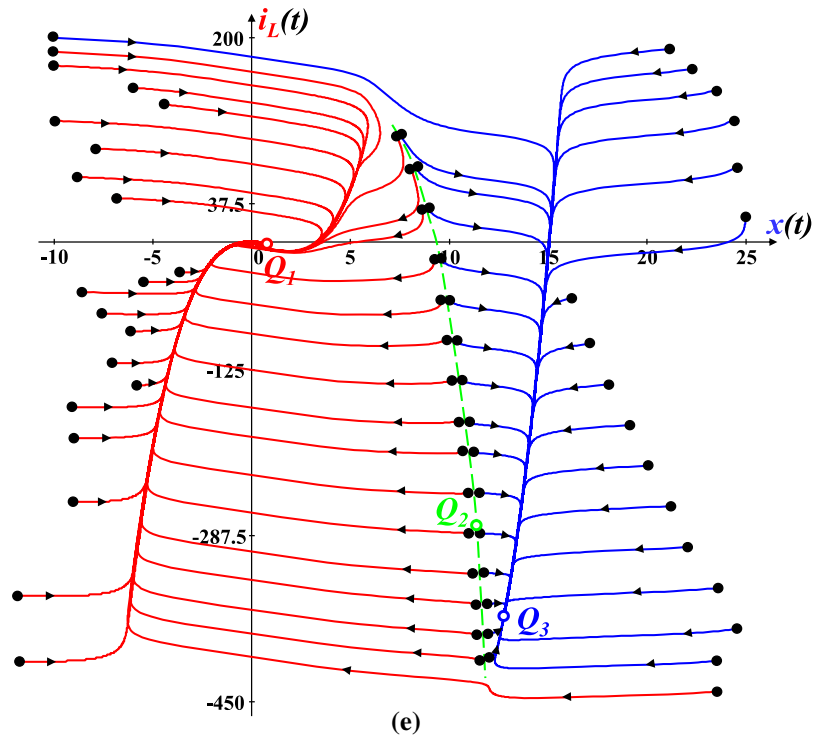
The four periodic steady-state responses of the state variable x , dubbed $x_a(t)$, $x_b(t)$, $x_c(t)$ and $x_d(t)$, of the CCM Circuit 3 in Figs. 20 and 21 exhibit four distinct types of stable *pinched hysteresis loops*. As an example, the blue pinched hysteresis loop for amplitude

$A = 1$ V, initial state $x(0) = 15.12$, and $f = 0.1$ Hz in Fig. 20b is spawned from the stable periodic steady-state response $x_b(t)$ of the state variable x , because the initial state $x(0) = 15.12$ falls within the basin of attraction $B_b(0)$ ($8.55 < x(0) \leq 24.55$), as specified in the inset in Fig. 20b. However, for any initial states $x(0) \leq 8.55$, or $x(0) > 24.55$, the state variable $x(t)$ of the CCM Circuit 3 converges to the stable periodic steady-state response $x_a(t)$, or $x_c(t)$, respectively, in Fig. 20b, because $x(0) \leq 8.55$ belongs to the *basin of attraction* $B_a(0)$, whereas $x(0) > 24.55$ falls in the *basin of attraction* $B_c(0)$. In contrast, any initial state

Fig. 19 Zoom view of the phase portrait in Fig. 18. **a** All red trajectories converge to the stable limit cycle corresponding to the repeller Q_1 , **b** all blue trajectories converge to the stable equilibrium point Q_3 , **c** all cyan trajectories converge to the stable equilibrium point Q_5 , **d** all green trajectories converge to the stable equilibrium point Q_7 . **e** Zoom view of the basins of attraction of the tiny stable limit cycle and stable equilibrium point Q_3 , respectively. The separatrix (passing through Q_2) of the basins of attraction of the small stable limit cycle surrounding the repeller Q_1 and the stable equilibrium point Q_3 is shown in green dashes



Basins of Attraction of stable limit cycle and stable equilibrium point Q_3



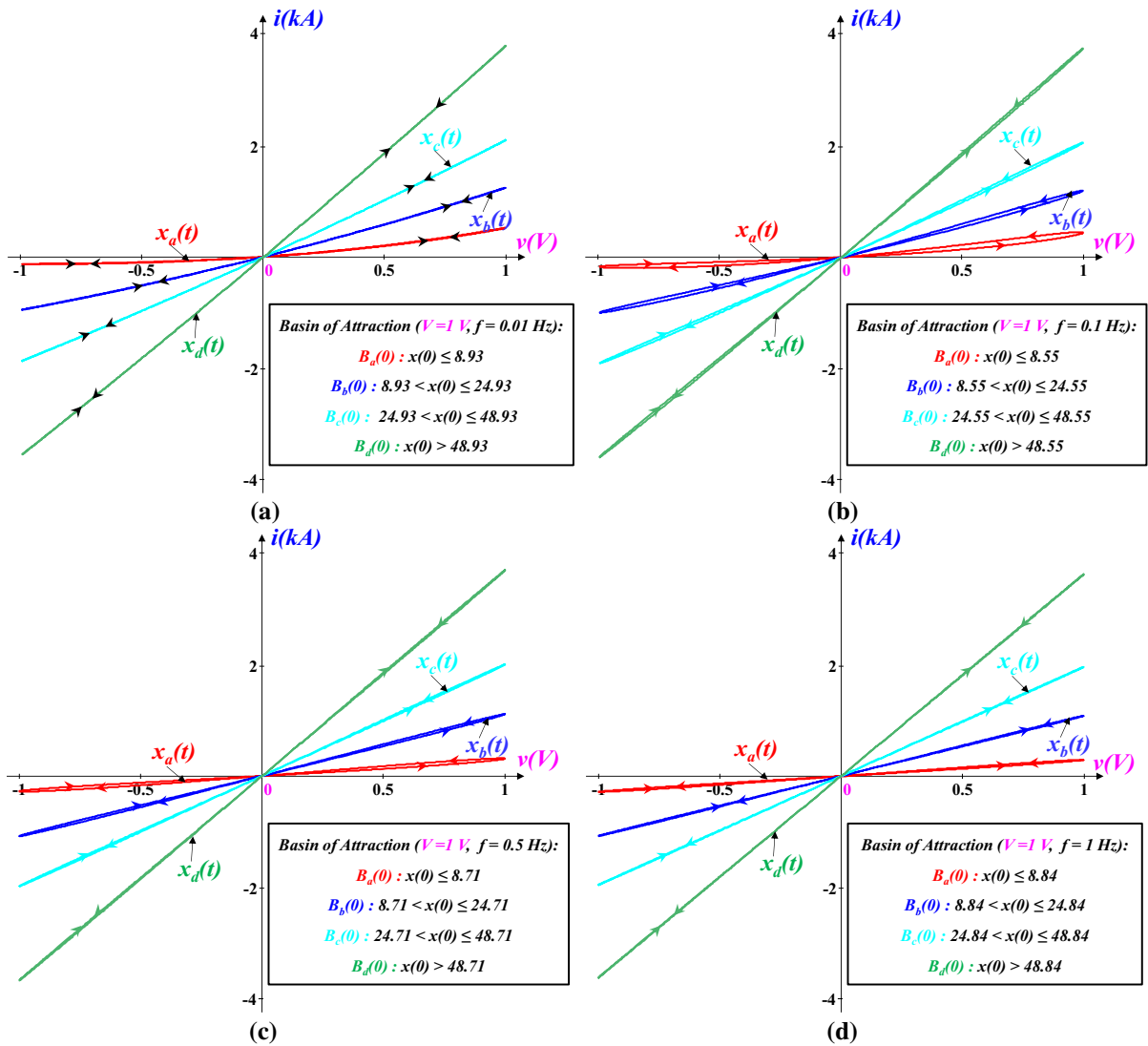


Fig. 20 The steady-state *pinched hysteresis loop* response $(i(t), v(t))$ of the *CCM Circuit 3* on the $i - v$ plane under AC periodic excitation $v_s(t) = A \sin(2\pi ft)$ where $A = 1\text{ V}$ and frequencies: **a** $f = 0.01\text{ Hz}$, **b** $f = 0.1\text{ Hz}$, **c** $f = 0.5\text{ Hz}$,

and **d** $f = 1\text{ Hz}$. For each frequency f , there exist *four* distinct basins of attraction, labeled as $B_a(0), B_b(0), B_c(0)$ and $B_d(0)$, for the corresponding *four* periodic steady-state state variable responses $x_a(t), x_b(t), x_c(t)$, and $x_d(t)$, respectively

$x(0) > 48.55$ belongs to the *basin of attraction* $B_d(0)$, which spawns the corresponding green *pinched hysteresis loop* in the $i - v$ plane shown in Fig. 20b.

Similarly, Fig. 21a–d shows four *pinched hysteresis loops* in the $i - v$ plane, spawned by four corresponding *stable* periodic steady-state responses $x_j(t)$ of the *CCM Circuit 3*. Their *basins of attraction* $B_j(0)$ are determined by the corresponding initial states $x_j(0)$, where $j \in \{a, b, c, d\}$.

All steady-state responses in Figs. 20 and 21 are *pinched hysteresis loops* passing through the origin, including those drawn as *single-valued curves* (in Figs. 20a and 21a) when their lobe areas are too small to discern. Moreover, observe that there exist *four* distinct stable steady-state responses $(x_a(t), x_b(t), x_c(t)$ and $x_d(t))$ for *sinusoidal excitation* just like the exist-

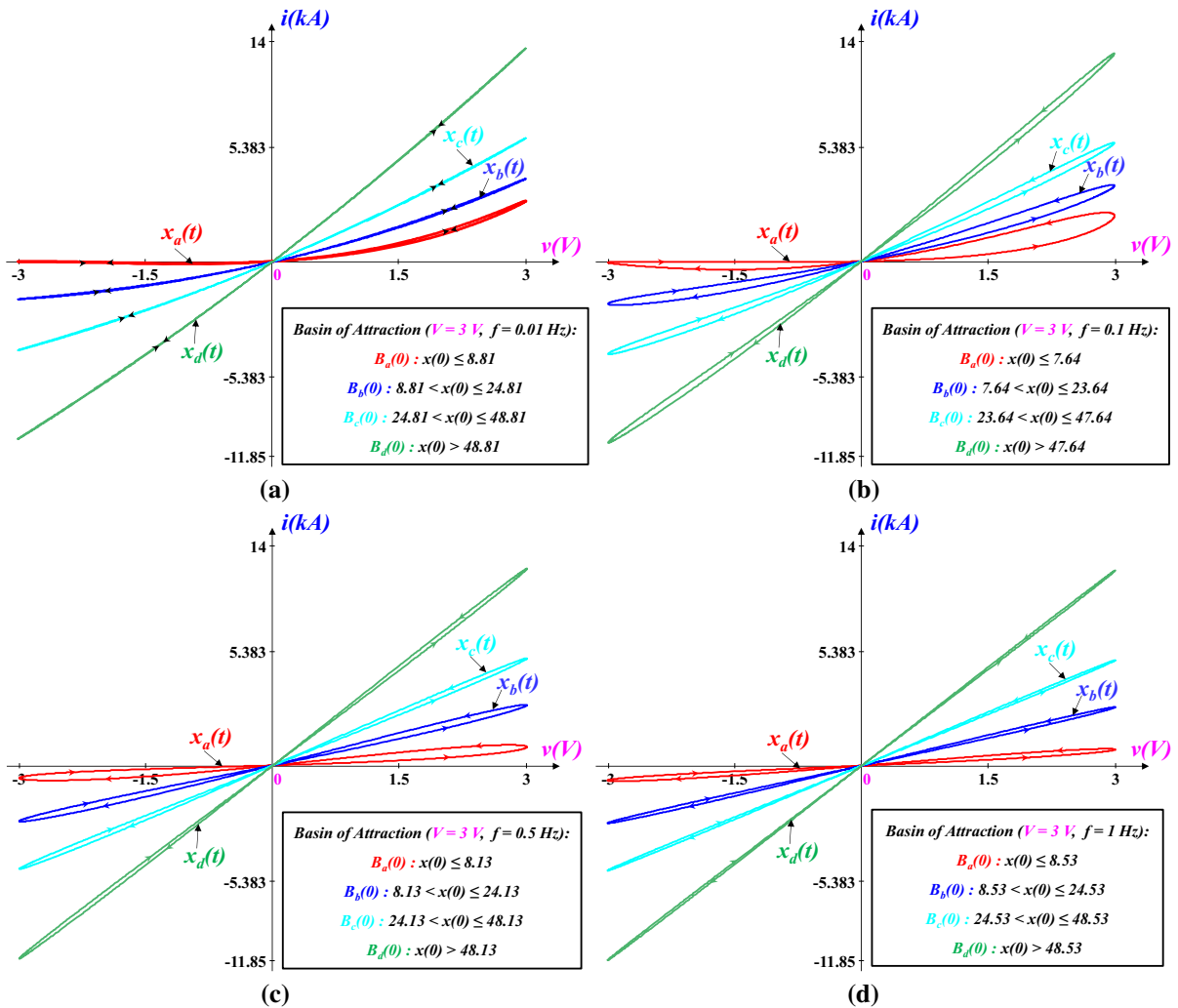


Fig. 21 The steady-state pinched hysteresis loop response ($i(t)$, $v(t)$) of the CCM Circuit 3on the $i - v$ plane under AC periodic excitation $v(t) = A \sin(\omega t)$ with $A = 3$ V and frequencies: **a** $f = 0.01$ Hz, **b** $f = 0.1$ Hz, **c** $f = 0.5$ Hz, and **d** $f = 1$ Hz.

Four distinct basins of attraction $B_j(0)$ of the state variables $x(t)$ and their corresponding initial states $x_j(0)$, $j \in \{a, b, c, d\}$, are listed in the inset of each figure

tence of *four* distinct equilibrium points (Q_1 , Q_3 , Q_5 and Q_7) under DC excitation⁸ (in Figs. 9a and 11a)

Since any initial state $x_j(0)$ originating from inside the *basin of attraction* $B_j(0)$ is attracted by a corresponding periodic steady-state response $x_j(t)$, the *stable* periodic steady-state responses $x_j(t)$ of the CCM Circuit 3 are called *dynamic attractors* in this paper. For each sinusoidal excitation, the one-dimensional basin

of attraction $B_j(0)$ of the four distinct dynamic attractors $x_j(t)$ is separated by *three* real numbers $x'(0)$, $x''(0)$, and $x'''(0)$, henceforth called *pinched hysteresis loop bifurcation points*. Each of the three bifurcation points depends on both the *amplitude* A , and the *frequency* f of the sinusoidal excitations, namely $x'(0) = F'(A, f)$, $x''(0) = F''(A, f)$, and $x'''(0) = F'''(A, f)$. For the convenience of readers, we include the heatmap, in Fig. 22, for specifying the bifurcation points (boundary points) separating the basins of attraction of the four dynamic attractors, $x_a(t)$,

⁸ Under DC steady state, the inductor L in CCM Circuit 2 is equivalent to a *short circuit*. In this case, from the circuit analysis perspective, the battery is directly connected across the CCM.

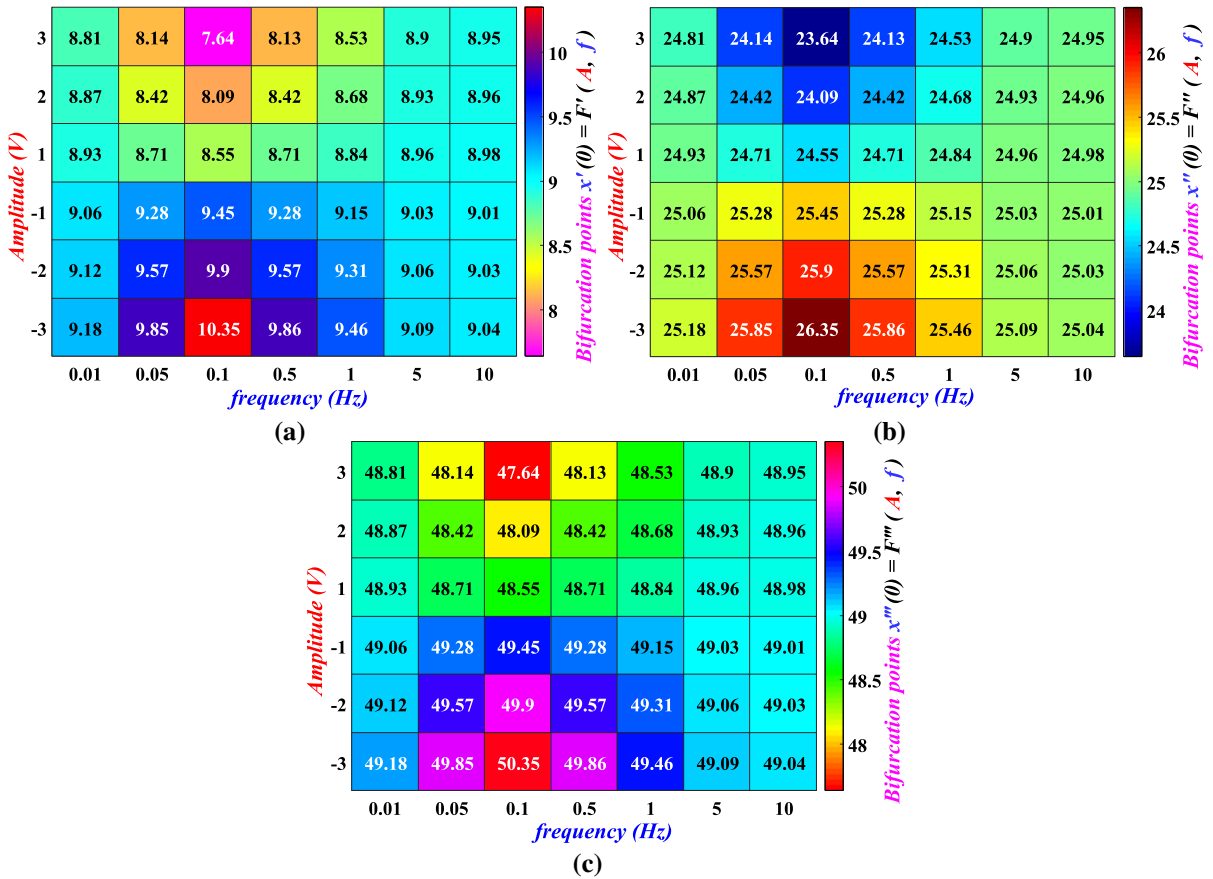


Fig. 22 The pinched hysteresis loop bifurcation points defining the basins of attraction of the dynamic attractors $x_a(t)$, $x_b(t)$, $x_c(t)$ and $x_d(t)$ of the CCM Circuit 3 for an input excitation $v(t) = A \sin(2\pi ft)$ in the amplitude–frequency plane. The heatmaps show **a** the bifurcation point $x'(0)$ specifying the

basins of attraction of the dynamic attractors $x_a(t)$, **b** the bifurcation point $x''(0)$ specifying the basins of attraction of the dynamic attractors $x_b(t)$, and **c** the bifurcation point $x'''(0)$ specifying the basins of attraction of dynamic attractors $x_c(t)$

$x_b(t)$, $x_c(t)$, and $x_d(t)$, of the CCM Circuit 3, for amplitudes $A \in \{-3, -2, -1, 1, 2, 3\}$ and frequencies $f \in \{0.01, 0.05, 0.1, 0.5, 1, 5, 10\}$. For example, the boundary points listed in the inset of Fig. 21 for $A = 3$ V are listed in Row 1 ($A = 3$) of Fig. 22a for $x_a(t)$, Fig. 22b for $x_b(t)$, and Fig. 22c for $x_c(t)$.

For example, Fig. 22a shows the periodic steady-state response $x(t)$ for a sinusoidal excitation⁹ with $A = -3$ V and $f = 0.1$ Hz converges to the dynamic attractor $x_a(t)$ for any initial states $x(0) \leq (x'(0) = F'(-3, 0.1) = 10.35)$ whereas for $x(0) > (x'(0) = 10.35)$, $x(t)$ converges to the dynamic attractor $x_b(t)$.

In contrast, any initial state ($x'(0) = 10.35 < x(0) \leq (x''(0) = F''(-3, 0.1) = 26.35)$), the steady-state response $x(t)$ of the CCM Circuit 3 exhibits the basin of attraction $B_b(0)$ corresponding to the dynamic attractor $x_b(t)$ shown in Fig. 22b, whereas for ($x''(0) = 26.35 < x(0) \leq (x'''(0) = F'''(-3, 0.1) = 50.35)$), $x(t)$ converges to the dynamic attractor $x_c(t)$ with corresponding basin of attraction $B_c(0)$ as shown in Fig. 22c. However, any initial states greater than the pinched hysteresis loop bifurcation points $x'''(0)$, i.e., $x(0) > (x'''(0) = F'''(A, f))$, the steady-state response $x(t)$ of the CCM Circuit 3 converges to the dynamic attractor $x_d(t)$ and exhibits the basin of attraction $B_d(0)$.

⁹ Negative amplitude A means $v(t) = -|A| \sin(2\pi ft)$, i.e., 180° out of phase from $v_s(t) = A \sin(2\pi ft)$.

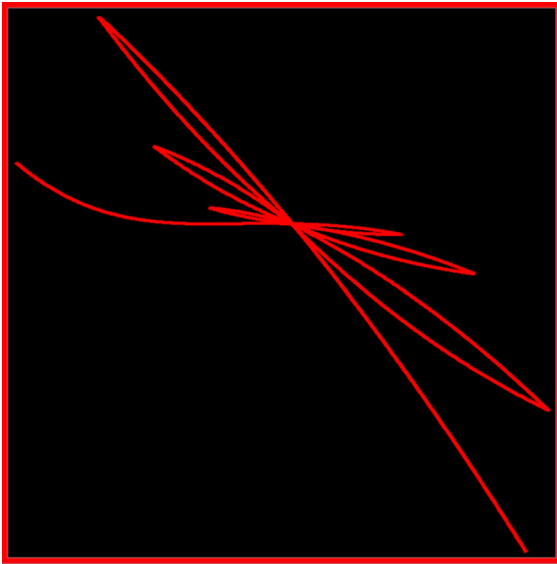


Fig. 23 Loci of the inverted DC V - I curve of the CCM, described analytically by two parametric equations $V = \hat{v}(x)$ and $I = \hat{i}(x)$ (Eqs. 10a and 10b). When the op-amp-based circuit realization of the CCM is measured experimentally using an oscilloscope, the dotted portion of the computed DC V - I curve in Fig. 7c cannot be seen without additional instrumentation because it represents unstable equilibrium points of the CCM circuit I in Fig. 2a, where the battery voltage is slowly tuned to cover the range $-10V < V < 10V$

7 Conclusion

This paper presents an in-depth global analysis of a three-element electronic oscillator circuit made of a Chua Corsage Memristor (CCM) connected in series with an inductor and a battery. The CCM can be built via a simple operational amplifier (op amp) circuit.

The CCM is a two-terminal electric device described by $i = x^2v$, where v and i denote the voltage and current of the device, respectively, and x is a state variable described by $dx/dt = f(x) + v$ where $f(x) = 33 - x + |x - 6| - |x - 12| + |x - 20| - |x - 30| + |x - 42| + |x - 56|$.

When connected in series with an inductor L with current i_L and a battery with voltage v , the Chua Corsage Memristor Oscillator is described by an autonomous system of two nonlinear ordinary differential equations (ODE)

$$\begin{aligned}
 dx/dt &= \left[\begin{array}{l} 33 - x + |x - 6| - |x - 12| + |x - 20| \\ - |x - 30| + |x - 42| - |x - 56| + i_L/x^2 \end{array} \right] \\
 &\triangleq f(x, i_L) \\
 di_L/dt &= 1/L^* (V - i_L/x^2) \triangleq g(x, i_L).
 \end{aligned}$$

When the CCM is connected directly (without the inductor) across a battery with voltage $v = V$, the resulting CCM circuit exhibits four stable equilibrium states $X(Q_1), X(Q_3), X(Q_5),$ and $X(Q_7)$ and three unstable equilibrium states $X(Q_2), X(Q_4),$ and $X(Q_6)$, located at the equilibrium points $Q_1, Q_3, Q_5,$ and $Q_7,$ and $Q_2, Q_4,$ and $Q_6,$ in the (x, \dot{x}) -plane, respectively.

Our first remarkable new results in this paper is to show that the DC V - I curve induced by the seven equilibrium states form a complicated but contiguous loci which can be expressed analytically by two exact explicit formulas $V = \hat{v}(X)$ and $I = \hat{i}(X)$, for $-\infty < X < \infty$.

Our next major result is to show that the second-order autonomous ODE can be designed into an oscillator with an appropriate choice of battery voltage $V = V^*$, and inductance $L = L^*$, by invoking the local activity principle. In particular, we derive a small subset of the two parameters (V, L) , dubbed the edge of chaos, via explicit analytical formulas. We analyze the edge of chaos domain and found systematically a parameter set (V^*, L^*) satisfying the supercritical Hopf bifurcation theorem, leading automatically to an electronic oscillator circuit, dubbed the CCM oscillator.

But the most exciting discovery of this paper is that when driven by $v = A \sin(2\pi ft)$, instead of the constant battery voltage $v = V$, the resulting non-autonomous ODE exhibits four distinct periodic solutions $x = \hat{x}(t)$, which induces four corresponding periodic currents $i = \hat{i}(t)$. When plotted in the current-vs.-voltage plane, the four periodic attractors induced four distinct coexisting pinched hysteresis loops, whose corresponding basins of attraction were precisely calculated.

The nonlinear dynamical theory presented in this paper can be easily generalized to design other second-order non-autonomous system of ODE with any finite number of coexisting attractors and their corresponding coexisting set of pinched hysteresis loops, which are the fingerprints of memristive systems endowed with memory, which are essential for designing learning machines.

We end this manuscript with the pinup portrait of a contiguous DC V - I Curve, redrawn in the $-I$ vs. V plane (shown in Fig. 23) of the Chua Corsage Memristor, which resembles a multi-lobe corsage ribbon.

Acknowledgements This work was supported in part by the National Research Foundation of Korea (NRF) grant funded by the Korea government (NRF-2019R1A2C1011297 and NRF-2019R1A6A1A09031717), US Air Force Office of Scientific Research under Grant number FA9550-18-1-0016, and research funds of Chonbuk National University in 2017.

Compliance with ethical standards

Conflict of interest The authors declare that they have no conflict of interest.

References

- Canete, J.F.D., Galindo, C., Moral, I.G.: System Description (ch. 3): System Engineering and Automation: An Interactive Educational Approach. Springer, Berlin (2011)
- Scott, A.C.: Nonlinear Biology (ch. 7): The Nonlinear Universe. Springer, Berlin (2007)
- Gintautas, V., Hübler, A.W.: Resonant forcing of nonlinear systems of differential equations. *Chaos* **18**(3), 033118 (2008)
- Kengne, J., Tabekoueng, Z.N., Tamba, K., Negou, A.N.: Periodicity, chaos, and multiple attractors in a memristor-based Shinriki's circuit. *Chaos* **25**(10), 103126 (2015)
- Mannan, Z.I., Choi, H., Kim, H.: Chua Cossage Memristor oscillator via Hopf bifurcation. *Int. J. Bifurc. Chaos* **26**, 1630009 (2016). <https://doi.org/10.1142/S0218127416300093>
- Mannan, Z.I., Choi, H., Rajamani, V., Kim, H., Chua, L.: Chua Cossage Memristor: phase portraits, basin of attraction, and coexisting pinched hysteresis loops. *Int. J. Bifurc. Chaos* **27**, 1730011 (2017)
- Mannan, Z.I., Yang, C., Kim, H.: Oscillation with 4-lobe Chua cossage memristor. *IEEE Circuits Syst. Mag.* **18**(2), 14–27 (2018)
- Kumar, S., Strachan, J.P., Williams, R.S.: Chaotic dynamics in nanoscale NbO₂ Mott memristors for analogue computing. *Nature* **548**, 318–321 (2017)
- Chen, M., Li, M., Yu, Q., Bao, B., Xu, Q., Wang, J.: Dynamics of self-excited attractors and hidden attractors in generalized memristor-based Chua's circuit. *Nonlinear Dyn.* **81**(1–2), 215–226 (2015)
- Bao, H., Park, J.H., Cao, J.D.: Adaptive synchronization of fractional-order memristor-based neural networks with time delay. *Nonlinear Dyn.* **82**(3), 1343–1354 (2015)
- Bao, H., Cao, J.D., Kurths, J., Alsaedi, A., Ahmad, B.: H ∞ state estimation of stochastic memristor-based neural networks with time-varying delays. *Neural Netw.* **99**, 79–91 (2018)
- Bao, H., Park, J.H., Cao, J.D.: Exponential synchronization of coupled stochastic memristor-based neural networks with time-varying probabilistic delay coupling and impulsive delay. *IEEE Trans. Neural Netw. Learn. Syst.* **27**(1), 190–201 (2016)
- Chua, L.: Resistance switching memories are memristors. *Appl. Phys. A* **102**, 765–783 (2011)
- Mannan, Z.I., Adhikari, S.P., Yang, C., Budhathoki, R.K., Kim, H., Chua, L.: Memristive imitation of synaptic transmission and plasticity. *IEEE Trans. Neural Netw. Learn. Syst. (Early Access)* **30**, 3458–3470 (2019)
- Mannan, Z.I., Yang, C., Adhikari, S.P., Kim, H.: Exact analysis and physical realization of the 6-lobe Chua Cossage Memristor. Complexity, Article ID-8405978, 1–21 (2018)
- Chua, L.: If it's pinched it's a memristor. *Semicond. Sci. Technol.* **29**, 104001-1-42 (2014)
- Chua, L.: Everything you wish to know about memristors but are afraid to ask. *Radio Eng.* **24**, 319–368 (2015)
- Chua, L.: Five non-volatile memristor enigmas solved. *Appl. Phys. A* **124**(563), 1–43 (2018)
- Roussel, M.R.: Stability Analysis for ODEs (ch. 3): Nonlinear Dynamics: A Hands-on Introductory Survey. Morgan & Claypool Publishers, San Rafael (2019)
- Sharov, A.: Stability, Oscillations and Chaos in Population Dynamics (ch. 9): Quantitative Population Ecology. Department of Entomology, Virginia Tech, Blacksburg, VA, USA <https://web.ma.utexas.edu/users/davis/375/popecol/lec9/equilib.html> (1996)
- Mainzer, K., Chua, L.: Local Activity Principle: The Cause of Complexity and Symmetry Breaking. Imperial College Press, London (2013)
- Chua, L.O.: Introduction to Nonlinear Network Theory. McGraw-Hill, New York (1969)
- Dogaru, R., Chua, L.O.: Edge of chaos and local activity domain of FitzHugh–Nagumo equation. *Int. J. Bifurc. Chaos* **8**, 211–257 (1998)
- Itoh, M., Chua, L.: Chaotic oscillation via edge of chaos criteria. *Int. J. Bifurc. Chaos* **27**, 1730035-1-79 (2017)
- Kuznetsov, Y.A.: Andronov: Hopf bifurcation. Scholarpedia. http://www.scholarpedia.org/article/Andronov-Hopf_bifurcation (2006)
- Strogatz, S.H.: Nonlinear Dynamics and Chaos, 2nd edn. Addison-Wesley Publishing Co., Boston (1994)
- Lynch, S.: Dynamical Systems with Applications using Maple™, 2nd edn. Birkhäuser, Berlin (2010)
- Layek, G.C.: An Introduction to Dynamical System and Chaos. Springer, New York (2015)
- Jordan, D.W., Smith, P.: Nonlinear Ordinary Differential Equations, 4th edn. Oxford University Press, Oxford (2007)
- Ascoli, A., Tetzlaff, R., Chua, L.O.: The first ever real bistable memristors—Part I: theoretical insights on local fading memory. *IEEE Trans. Circuits Syst.* **II**(63), 1091–1095 (2016)
- Ascoli, A., Tetzlaff, R., Chua, L.O.: The first ever real bistable memristors—Part II: analysis of a local fading memory. *IEEE Trans. Circuits Syst.* **II**(63), 1096–1100 (2016)

Publisher's Note Springer Nature remains neutral with regard to jurisdictional claims in published maps and institutional affiliations.